

ARMY RESEARCH LABORATORY



# Laser Simulation of Single-Event Effects: A State of the Art Review

by Stephen Buchner

ARL-CR-185

March 1995

prepared by

Martin Marietta Research Laboratories  
1450 S. Rolling Road  
Baltimore, MD 21227

under contract

N00014-90-2231



This work was sponsored by the Defense Nuclear Agency under work unit 00036,  
Radiation-Hardened Microelectronics.

19950321 018

DEFENSE QUALITY INSPECTION REPORT

Approved for public release; distribution unlimited.

The findings in this report are not to be construed as an official Department of the Army position unless so designated by other authorized documents.

Citation of manufacturer's or trade names does not constitute an official endorsement or approval of the use thereof.

Destroy this report when it is no longer needed. Do not return it to the originator.

<b>REPORT DOCUMENTATION PAGE</b>			Form Approved OMB No. 0704-0188	
Public reporting burden for this collection of information is estimated to average 1 hour per response, including the time for reviewing instructions, searching existing data sources, gathering and maintaining the data needed, and completing and reviewing the collection of information. Send comments regarding this burden estimate or any other aspect of this collection of information, including suggestions for reducing this burden, to Washington Headquarters Services, Directorate for Information Operations and Reports, 1215 Jefferson Davis Highway, Suite 1204, Arlington, VA 22202-4302, and to the Office of Management and Budget, Paperwork Reduction Project (0704-0188), Washington, DC 20503.				
1. AGENCY USE ONLY (Leave blank)		2. REPORT DATE March 1995		3. REPORT TYPE AND DATES COVERED Final, August 1990 to August 1993
4. TITLE AND SUBTITLE Laser Simulation of Single-Event Effects: A State of the Art Review			5. FUNDING NUMBERS Contract No: N00014-90-2231 Program El: 62120	
6. AUTHOR(S) Stephen Buchner				
7. PERFORMING ORGANIZATION NAME(S) AND ADDRESS(ES) Martin Marietta Research Laboratories 1450 S. Rolling Road Baltimore, MD 21227			8. PERFORMING ORGANIZATION REPORT NUMBER ARL-CR-185	
9. SPONSORING/MONITORING AGENCY NAME(S) AND ADDRESS(ES) Defense Nuclear Agency 6801 Telegraph Road Alexandria, VA 22310-3398			10. SPONSORING/MONITORING AGENCY REPORT NUMBER	
11. SUPPLEMENTARY NOTES AMS code: 612120.H250000      This work was sponsored by the Defense Nuclear Agency under ARL PR: 324228      work unit 00036, Radiation-Hardened Microelectronics. ARL contact: Harvey Eisen or Timothy Oldham				
12a. DISTRIBUTION/AVAILABILITY STATEMENT Approved for public release; distribution unlimited.			12b. DISTRIBUTION CODE	
13. ABSTRACT (Maximum 200 words)  A pulsed laser system for simulating heavy-ion, single-event effects in semiconductor devices is described. The fundamentals of ion and laser interactions in silicon are compared. The results of several case studies demonstrate the utility of the laser technique for both hardness assurance and diagnostic purposes.				
14. SUBJECT TERMS Single-event upsets (SEUs), laser simulation, single-event effects (SEEs)			15. NUMBER OF PAGES 57	
			16. PRICE CODE	
17. SECURITY CLASSIFICATION OF REPORT Unclassified	18. SECURITY CLASSIFICATION OF THIS PAGE Unclassified	19. SECURITY CLASSIFICATION OF ABSTRACT Unclassified	20. LIMITATION OF ABSTRACT UL	

# Contents

1. Introduction .....	5
2. Pulsed Laser Applications .....	10
2.1 Hardness Assurance .....	10
2.2 Diagnostic Tests .....	11
3. Comparison of Ion and Laser-Induced Upsets .....	14
3.1 Ion Charge Tracks .....	14
3.2 Laser Charge Tracks .....	15
3.3 Funneling .....	17
3.4 Shunt Effect .....	18
3.5 Carrier Lifetime .....	18
3.6 Diffusion .....	19
3.7 Generation Time .....	20
3.8 Reflections .....	20
3.9 Cross-Section .....	21
3.10 Nonlinear Effects .....	21
3.10.1 Two-Photon Absorption .....	22
3.10.2 Free-Carrier Absorption .....	22
3.10.3 Bandgap-Narrowing .....	23
3.10.4 Lattice Heating .....	24
3.11 Calculation of Laser LET .....	24
4. Equipment and Procedure .....	26
4.1 Equipment .....	26
4.2 Test Procedure .....	33
4.3 System Automation .....	34
5. Correlation and Calibration .....	35
5.1 Correlation .....	35
5.2 Calibration .....	37
6. Case Studies .....	38
6.1 64K SRAM .....	39
6.1.1 Upset Threshold Measurements .....	39
6.1.2 Spatial Effects .....	40
6.1.3 Multiple Upsets .....	41
6.1.4 Timing Effects .....	41
6.2 GaAs Logic Circuit .....	42
6.3 SA3300 Microprocessor .....	44
6.4 Spatial Variation in Upset Threshold .....	46
7. Lessons Learned .....	49
8. Perspectives .....	50

Accession For	
NTIS	CRA&I <input checked="" type="checkbox"/>
DTIC	TAB <input type="checkbox"/>
Unannounced <input type="checkbox"/>	
Justification	
By	
Distribution /	
Availability Codes	
Dist	Avail and/or Special
A-1	

## Contents (cont'd)

<b>9. Conclusions and Recommendations .....</b>	<b>51</b>
9.1 <i>Conclusions</i> .....	51
9.2 <i>Recommendations</i> .....	51
<b>10. References .....</b>	<b>52</b>
<b>Distribution .....</b>	<b>55</b>

## Figures

1. Radial charge density profile for 1-GeV Fe ion and pulsed laser beam at distance of 0.125 m below surface .....	16
2. Shape of focused laser beam passing from air to SiO <sub>2</sub> and then Si. ....	17
3. Absorption coefficient for Si as function of photon energy .....	23
4. Schematic of equipment needed for pulsed laser SEE testing .....	26
5. Energy dependence of absorption coefficients for both <i>n</i> - and <i>p</i> -type GaAs as function of doping .....	29
6. Layout of SRAM cell .....	40
7. Bitmap showing addresses of cells surrounding cell 3724 .....	41
8. Schematic of one pipeline register designed for SEU immunity .....	43
9. Relative upset threshold as function of delay between arrival of laser pulse and arrival of clock for three nodes of pipeline register .....	44
10. Schematic of register for SA3300 microprocessor .....	45
11. Distribution of upset threshold for 93L422 .....	47
12. Cross-section as function of LET for 93L422, showing gradual rise of cross-section with LET .....	47
13. Distribution of upset thresholds for HM6504RRH SRAM .....	48

## Tables

1. Values used in calculation of LET .....	25
2. List of equipment needed for SEE testing .....	26
3. Upset and latchup thresholds for memory cells .....	35
4. Published upset and latchup LET values .....	37
5. Comparison of ion and laser upset values .....	37
6. Ion and laser upset LETs for two bipolar devices .....	37
7. Relative upset thresholds for transistors in four different cells in 64K SRAM .....	39
8. Spatial and data dependence of upsets for two cells .....	40
9. Upset thresholds (MeV-cm <sup>2</sup> /mg) for ion and laser tests .....	46

# 1. Introduction

Single-event effects (SEEs) occur when energetic ions pass through sensitive nodes of integrated circuits, causing a loss of information that can have serious consequences for the performance of a space system. SEEs in integrated circuits consist of both single-event upsets (SEUs) and single-event latchups (SELs). In the case of SEUs, the information is corrupted by the ion, but there is generally little or no permanent damage to the circuit. Single-ion total-dose effects have been reported [1,2], but they are not common. Generally, the circuit can continue to operate properly once the upset has been detected and corrected. Typically, only after many ions have struck the same region of the circuit does damage affect the circuit's operation. SEL manifests itself as increased current flow and stuck bits that may lead to circuit damage. If no permanent damage has occurred, SEL can be corrected by removing power from the system and then turning it back on.

Special technologies and circuit designs are used to improve a circuit's immunity to SEE. For instance, silicon-on-insulator technology hardens a circuit's immunity to SEU by limiting the amount of charge collected at a sensitive node. It also avoids the problem of SEL altogether. Other approaches aimed at reducing a circuit's sensitivity to SEU include adding cross-coupled resistors, capacitors, or transistors to increase the time constants.

Clearly, there is a need for testing to verify the SEE immunity of new designs. There is also a need for nondestructive testing of devices that will actually be used in a system to ensure SEE hardness. Finally, if unforeseen SEE phenomena occur, a method for identifying their origins would be essential for their understanding and elimination.

Accelerator testing, where the circuit is exposed to an ion beam, is the currently accepted method for measuring SEE vulnerability. Circuits are characterized for their SEE sensitivity by measuring the cross-section as a function of accelerator ion linear energy transfer (LET). In the ideal case where the sensitive volumes in the circuit are parallelepipeds with large lateral dimensions and small depths, the cross-section versus LET curve should exhibit a step function at a value of LET for which charge equal to the critical charge is deposited in the sensitive volume. In many cases, the cross-section rises gradually with LET, saturating only at very high values of LET. By performing a convolution of the cross-section versus LET curve with models of the radiation environment, one can calculate error rates. There are, however, certain limitations associated with routine ion-beam testing:

*Limited access.* Relatively few facilities are available for SEE testing, and existing facilities are heavily used, leading to significant delays.

*Damage to the circuit.* The ion beam is destructive, imparting damage to the circuit that ultimately limits its useful life. Damage by single ions is becoming more important as the size of the individual transistors decreases.

*Inconvenient.* Ion-beam testing is inconvenient for two reasons: (a) the devices must be tested in a vacuum, and (b) the accelerator is typically located far from the chip manufacturer or user.

*Lack of spatial and temporal data.* Of paramount importance for diagnostic applications are spatial and temporal information regarding the origin of SEE. Unfortunately, most ion-beam facilities are not set up to do spatial measurements, and temporal measurements are even more difficult to do.

*Expense.* Beam time is expensive, costing from \$600 an hour at Brookhaven National Laboratory (BNL), including setup time, to thousands of dollars per hour at the Berkeley Bevatron.

*Inability of ions to penetrate thick dielectric layers.* Some chips, such as those used in multichip modules, are protected by thick dielectric layers that prevent low-energy ions from producing upsets. For SEE testing of these devices, it is necessary to go to high-energy accelerators such as the Berkeley Bevatron or GANIL in France, where the costs are high and the access more limited.

*Track structure differences.* High-energy cosmic rays produce charge tracks with much larger diameters than the relatively low-energy ions available at accelerators such as BNL. For example, charge collection efficiency from charge tracks generated by ions with different energies (395 MeV and 25 MeV Cu ions) and the same LET (26 MeV-cm<sup>2</sup>/mg) have been modeled using a computer and are quite different, because of effects such as Auger recombination and funneling, which depend on track charge density [3]. Evidently, low-energy accelerator ions are an approximation to cosmic ray ions, although the exact role played by track structure is not yet well understood, particularly in light of the fact that error-rate predictions using cross-section versus LET curves for devices with relatively large dimensions agree quite well with actual upset rates measured in space. However, as the dimensions of transistors decrease, the charge track size is expected to play a more important role in determining upset threshold. Low-energy accelerator ions may not then accurately simulate the effects of cosmic rays.

Two alternate techniques that have been proposed for SEE testing are a pulsed laser and californium (<sup>252</sup>Cf). Both are being developed because it is hoped that, although accelerator testing will always be required, the use of the alternative method will reduce the amount of accelerator testing required to screen and characterize devices.

<sup>252</sup>Cf decays spontaneously, producing a spectrum of high-energy particles with energies centered around 102.5 and 78.7 MeV and with mean masses of 106.2 and 142.2 amu, respectively, as well as alpha particles and fast neutrons. However, the range of the fission ions is small in silicon because of their low energy and large LET. In fact, it has been shown that <sup>252</sup>Cf does not always give reliable results for SEL, as the ions do not penetrate sufficiently far into silicon to trigger latchup [4]. In contrast, the energetic heavy ions in space typically go right through the circuit and easily

cause latchup. A major disadvantage of  $^{252}\text{Cf}$  is its radioactivity, which requires special safety precautions for health reasons. In this report we will not discuss further the role of  $^{252}\text{Cf}$  in SEE testing.

An ion produces an upset in a circuit if the charge generated by the ion and collected at a sensitive node exceeds the critical charge for that node. Laser light can also generate upsets in circuits, provided the photon energy is larger than the energy of the semiconductor bandgap. Under those conditions, the laser light is absorbed by the semiconductor, producing a track of charge (electron-hole pairs). The pulsed laser offers the following advantages for SEE testing:

*Nondestructive.* As long as the intensity is below that which produces melting in the semiconductor, there is no permanent damage to the material by the laser light. All devices with upset threshold LETs below  $200 \text{ MeV-cm}^2/\text{mg}$  that were tested with the laser required energies at most about two orders less than that required to damage the material. Hence, the technique is perfectly suited for both hardness assurance measurements and for detailed investigations of effects that require many hits to a single area of a transistor, such as in charge-collection measurements from test structures. The technique can also be used to prescreen circuits to make sure they are operating properly prior to traveling to an accelerator facility, where improperly operating circuits could cause delays and additional expense.

*Relatively inexpensive.* The technique is relatively inexpensive, as the laser, optical system, and vibration isolation table can all be purchased for about \$150K. Test equipment for monitoring upsets is not included in the above estimate because it is also used for accelerator testing.

*Convenient.* The technique is convenient because it is totally compatible with a fabrication facility. There is no ionizing radiation threat, and the entire system can be enclosed in a light-tight box to avoid the possibility of eye damage. No vacuum is required for testing; the LET can be changed merely by changing the intensity of the light, and setup time is very short.

*Capable of providing spatial information.* Because the laser light can be focused down to a small spot and positioned on a particular transistor, the sensitivities of individual transistors can be measured. For instance, in testing a static random-access memory (SRAM) HM6504 for latchup, we found that the peripheral circuitry was four times more sensitive to latchup than the memory cells. Therefore, to reduce the latchup sensitivity of the device, the peripheral circuitry should be hardened rather than the cells themselves [5].

*Capable of providing temporal information.* By synchronizing the laser to the circuit clock, we were able to measure the timing dependence of upsets in a logic circuit. If the pulse of laser light arrived at a particular gate just as the clock voltage was switching from low to high, an upset would occur. If the light arrived after the clock voltage had already switched, no upset would occur. If it arrived before the clock signal, an upset could occur, but only at a higher laser energy. In fact, the energy required to produce an

upset depended on the length of the time interval between the arrival times of the laser light and the clock. The greater that time interval, the more energy was required to produce the upset. Thus, there is an upset window whose width depends on the LET of the ions. This kind of data has not been obtained with an accelerator, and it illustrates how useful the laser is for investigating SEE in logic circuits [6].

*LET threshold determination.* In contrast to ion-beam testing, it is a simple matter to determine the upset threshold with a pulsed laser. Simply by changing the intensity of the light, we can vary the LET and determine the threshold.

*Adjustable range.* Energetic ions in space pass right through a circuit, producing a very long track of charge. In contrast, low-energy accelerator ions penetrate a relatively short distance into the semiconductor. The range plays a role in charge collection by devices manufactured in bulk silicon, but should be less important for devices manufactured in thin epitaxial layers, provided the range is greater than the thickness of the epitaxial layer. The range of the laser light can easily be adjusted by changing its wavelength. For instance, when devices are being tested on thin epitaxial layers, it is not necessary to select light that penetrates to distances of hundreds of microns.

*Accelerator beam costs and facility scheduling.* Substitution of laser testing and screening, as appropriate, will eliminate the high rental costs and scheduling problems associated with accelerator testing.

The technique is not without its own limitations. They include:

*No absolute measure of SEE threshold.* Because light and ions do not interact in the same way with the semiconductor, there are significant differences in track structure. The laser produces a charge track with a Gaussian radial profile that decays exponentially and spreads out with distance from the surface. In contrast, the radial charge density profile of the track generated by the ion is much more sharply peaked at its center, does not decay exponentially, and does not spread out with distance from the surface. Differences in track structure are expected to manifest themselves as differences in measured LET upset thresholds. How the differences are expected to affect the measurements of the upset threshold will be described in greater detail in section 3.

*No direct measure of the cross-section.* To calculate error rates, the variation of the cross-section with LET must be measured. Using only the threshold LET and the limiting cross-section, one may overestimate the error rate by up to an order of magnitude. One can use the laser to obtain the limiting cross-section indirectly by identifying which nodes are sensitive to upset and then using the circuit layout to add up all the sensitive areas. This method will also be described in section 3.

*Inability of the light to penetrate metal.* An ion will pass through metalization, but laser light will not. For instance, in some devices, such as the 93L422

256 × 4 bipolar SRAM, the upset threshold varies across the surface of the sensitive volume. If the most sensitive region that corresponds to the threshold is covered by metal, the laser will be unable to measure the threshold. The problem is exacerbated in devices where the sensitive nodes are completely covered by metal. As more and more transistors are incorporated on a single chip, greater use will be made of multilevel interconnects that cover SEE-sensitive areas on the chip. This will severely limit the usefulness of the technique with regard to measuring upset threshold.

Clearly, there are both advantages and limitations to the pulsed laser technique. However, on balance, it is a useful technique for SEE hardness assurance testing and for diagnostic purposes. It will not replace ion-beam testing, but it will be a complementary technique that will assist in characterizing SEE in circuits.

## 2. Pulsed Laser Applications

The pulsed laser can be used for SEE hardness assurance testing, for diagnostic probing, and for testing circuits that cannot readily be tested with an ion beam, such as multichip modules covered with a thick dielectric layer. It also has great potential for testing SEE in microprocessors, because both spatial and temporal information is required to evaluate a microprocessor's SEE sensitivity.

### 2.1 Hardness Assurance

SEE hardness assurance involves measuring either every circuit or at least a representative number of circuits or test structures to ascertain whether they meet SEE specifications. At present, if done at all, hardness assurance is only carried out on a few representative circuits at an accelerator facility using ions that produce a small but finite amount of damage to the circuit. The availability of a nondestructive, convenient, inexpensive, and rapid test for hardness assurance is an attractive prospect because it would make possible the testing of large numbers of circuits.

The pulsed laser technique is nondestructive provided that (1) the pulse energy needed to produce an upset is less than that required to damage the semiconductor by melting, and (2) the photon energy is less than that needed for photon-assisted tunneling of charge from the semiconductor into the oxide, where the charge can become trapped and alter the operating parameters of the circuit. In most cases measured to date, even for hardened devices with threshold LETs of approximately  $100 \text{ MeV-cm}^2/\text{mg}$ , the energy needed to produce an upset is smaller than that needed to melt the semiconductor. Also, the photon energy ( $<2 \text{ eV}$  for Si) and the electric fields applied are sufficiently small that negligible charge is injected via photon-assisted tunneling.

For hardness assurance, the laser beam is focused to a spot with a diameter on the order of a micron, such that only a single transistor is probed at any one time. The upset threshold for that particular transistor can be measured, but it may not represent the true upset threshold for the circuit. For example, it has been reported that SRAM cells hardened with decoupling polysilicon resistors have a wide distribution of upset thresholds caused by a large, process-related variation in the resistivity of the polysilicon resistors [7]. For this case, it is obviously necessary to measure a statistically significant number of cell upset thresholds to obtain a measure of the overall SEE sensitivity. More recent experiments with the pulsed laser demonstrate that the cell-to-cell upset threshold does not vary significantly, even for memories with decoupling resistors [8]. (Apparently, processing-related variations in resistor values have been corrected.)

Using the pulsed laser, we were able to show that the upset threshold varies with position in the sensitive areas of a memory cell, such as the drain of an "off" transistor. Therefore, when memories are being tested, with a

pulsed laser it is necessary to position the laser spot in exactly the same relative location in each cell. Since only the relative upset thresholds are important, it is best to select a location at which the upset threshold is a minimum, because that will simplify locating the same relative spot in each cell.

Obviously, any variations in the upset threshold measured across the wafer should be due to variations in actual SEE threshold rather than variations in other factors, such as the amount of light available for producing upsets. For instance, variations in the openings in metal contacts on top of sensitive drains that are due to poor control during processing can affect the amount of light available for producing upsets. For large-area devices this has not been a problem. However, for devices with critical dimensions equal to or smaller than the diameter of the focused laser spot, this may in fact become a problem.

An important point regarding hardness assurance testing with the laser that needs stressing is that it is not necessary that the laser and ion LET upset thresholds give exactly the same value, provided that (1) the relative numbers agree and (2) a fiduciary set of measurements exists for that type of circuit, comparing ion and laser upset thresholds. For example, by testing a particular SRAM for SEE sensitivity with both an ion beam and a pulsed laser, the laser upset threshold can be directly compared with the ion beam upset threshold. All subsequent measurements can then be done with the laser. Any variations in SEE threshold can be referred to the ion data for absolute values, provided, as pointed out previously, the variations are not due to effects unique to the laser measurements.

Once the initial investment has been made in setting up the system, the cost of testing the circuits is not large, especially if the testing is automated.

## **2.2 Diagnostic Tests**

For SEU diagnostic testing, it is essential to be able to locate the origins of upsets in both space and time. The pulsed laser is ideal for that task because the light can be focused down to a small spot and used to identify SEE-sensitive transistors. It is possible to measure the dependence on time of the upset sensitivity by synchronizing the circuit clock with the firing of the laser, and introducing a delay between the clock signal and the arrival time of the laser. Those transistors found to be particularly susceptible to upsets can be redesigned for greater immunity.

When a pulsed laser is used for diagnostic tests, it is usually not necessary to measure upset threshold accurately. A ballpark figure is frequently sufficient, because faulty designs usually result in large changes in SEE threshold. For instance, we tested a series of registers in a GaAs logic circuit designed to be immune to SEU and discovered that some designs were quite sensitive, while others were immune. This was of invaluable assistance to the designers in selecting the design that offers the most immunity to SEU.

An important application for the pulsed laser is the generation of SRAM bit maps, which are frequently not available from manufacturers. Bit maps are particularly helpful in understanding multiple bit upsets. For example, we tested a 93L422 circuit that failed even though error detection and correction (EDAC) had been implemented to protect against SEU. From the bit map we were able to show that certain bits from the same word were located physically adjacent to one another. A single ion incident between the two cells could upset two bits in the same word, which could not be corrected by the EDAC code. As long as there is some small space open on the surface of the chip to allow the light to reach the silicon, it should be possible to upset internal nodes and check to see whether the EDAC is working. This is particularly important in sensitive devices such as dynamic random-access memories (DRAMs), where a single ion can produce upsets in many adjacent cells. By increasing the intensity of the laser pulse until EDAC fails, one can estimate how well EDAC will work in a particular radiation environment. EDAC validation experiments are currently being planned on 4-Mbit DRAMs that have very low upset thresholds.

Accurate values for upset thresholds cannot be obtained with the pulsed laser for totally new designs. A fiduciary value must first be obtained from ion-beam testing for calibration purposes. The effect on SEE sensitivity of minor design modifications to a circuit previously tested with both ion and laser beams can be evaluated with a laser beam, thereby avoiding the necessity of repeating accelerator testing.

Multichip modules cannot be tested at most accelerators because the dielectric layer that covers the chip is too thick for the relatively low-energy ions to penetrate. SEE testing, therefore, must be carried out before the chip has been incorporated into the multichip module package at places such as the Berkeley Bevatron, Chalk River, or GANIL. Because some of the dielectrics, such as Kapton, are transparent, the laser light is able to reach the circuit. Pulsed-laser testing has been used successfully to investigate SEE phenomena in multichip modules.

Another application for the pulsed laser is software validation. Rather than having to correct software during a run at an accelerator where costs are considerably higher, one can use the pulsed laser to check the software before the accelerator testing. In one case we tested a particularly SEE-sensitive gate array by irradiating the entire circuit with a defocused beam and maximum laser energy. Two different codes were tested, and the most suitable one for accelerator testing was identified.

Recent results by Kim et al. [9] confirm that the laser can, under certain conditions, be used as an inexpensive laboratory SEU prescreen tool. They found good agreement between the laser and ion-beam upset thresholds for two 64K SRAMs. The good agreement is fortuitous, as our results on a 64K SRAM suggest, because effects such as funneling (to be discussed in the next section) are quite different for laser light and for ions. To have confidence in these measurements, one must first compare ion and laser upset thresholds experimentally to establish a valid fiduciary mark. Then,

all subsequent laser measurements on the same type of device can be compared to the fiduciary value to establish an accurate absolute upset threshold.

Charge-collection measurements on test structures are invaluable in understanding the physics of SEU. The great advantage of the laser for doing charge-collection measurements is that the light does not damage the semiconductor, making it possible to capture charge-collection waveforms using sampling oscilloscopes. Ions, on the other hand, damage the circuit and, after a finite dose, the shape of the charge collection pulse changes. Convenience is another factor that makes charge-collection measurements with a pulsed laser an attractive alternative to ion-beam experiments.

### 3. Comparison of Ion and Laser-Induced Upsets

In this section we will compare charge-collection mechanisms for laser light and ion-generated charge tracks across semiconductor junctions. We will show that differences in the threshold LETs measured by the two methods are due to differences in the track structures. The laser-generated charge track is much wider than the ion-generated charge track and spreads out laterally as it propagates through the semiconductor. However, in spite of these differences, a pulsed laser can still be used for investigating SEE phenomena because relative upset values can be measured. Pulsed laser testing can be used primarily as a diagnostic tool or as a way of assuring SEE hardness. It cannot be used to measure absolute upset thresholds because the upset energy does not correspond exactly to ion LET for a variety of reasons specified in subsequent sections. Pulsed-laser testing will not eliminate the need for ion-beam testing. Its role in SEE testing will be to complement that of ion-beam testing, particularly in the areas of hardness assurance and diagnostic evaluation, thereby reducing the amount of ion-beam testing.

#### 3.1 Ion Charge Tracks

When a cosmic ray ion passes through a semiconductor, it loses energy by ionizing (electron-hole ( $e-h$ ) pair generation) and non-ionizing (lattice damage) processes. The energy lost per unit length to ionization divided by the material density is defined as the LET, and has been tabulated for different ions as a function of their energy. To calculate the amount of charge generated requires information on both the variation of the ion's LET with distance along the track and the energy it takes, on average, to produce one  $e-h$  pair (3.6 eV in Si). Energy lost in "dead" layers, such as passivation layers, must also be considered.

The amount of collected charge is more difficult to calculate. A first-order approximation is obtained by taking the product of the LET and the width of the depletion layer. However, effects such as funneling and recombination (to be described in greater detail later) complicate the process.

In contrast to the relatively uniform charge density along the axis of the ion-generated charge track, the radial density is strongly peaked at the track's center and falls off rapidly with distance. Low-energy ions have track diameters from about 0.1 to 0.5  $\mu\text{m}$ , whereas heavy energetic ions (GeV) found in cosmic rays have much larger tracks with diameters of up to 3  $\mu\text{m}$ . Using a program called TRKRAD, based on a theory of Kobetich and Katz, charge densities at the center of the track approach  $10^{23} \text{ cm}^{-3}$ , much larger than the carrier densities in doped regions of typical semiconductor devices [10].

### 3.2 Laser Charge Tracks

The interaction of light with the semiconductor depends on the energy of the photon relative to that of the bandgap of the semiconductor which, in the case of Si, is 1.1 eV. For photon energies smaller than the bandgap energy, the light passes unattenuated through the semiconductor, except for reflections from the surfaces. When the photon energy is larger than the bandgap energy, the light is absorbed and its amplitude decreases exponentially with distance from the surface (Beer's law). By choosing the photon energy close to that of the bandgap (where the absorption is small), the penetration depth can be made large. Under those conditions, the charge density in the vicinity of the junction, just as in the case of a track produced by a heavy ion, does not change much with distance. One can then use a linear approximation to the exponential decay in the vicinity of the junction to calculate the amount of charge generated per unit length.

Under certain circumstances it is advantageous to choose light with photon energy significantly greater than the silicon bandgap, where the absorption is large. For instance, at 800 nm, the absorption coefficient is  $720 \text{ cm}^{-1}$ , giving a penetration depth of only  $14 \text{ }\mu\text{m}$ . Most current devices are manufactured in thin (approximately  $10 \text{ }\mu\text{m}$  thick), epitaxial silicon layers grown on highly doped substrates. Very little charge is collected from the substrates because of the very short minority carrier lifetime in highly doped semiconductor regions. Thus, the light need only have a penetration depth comparable to the thickness of the epitaxial layer. These results have been confirmed by computer modeling.

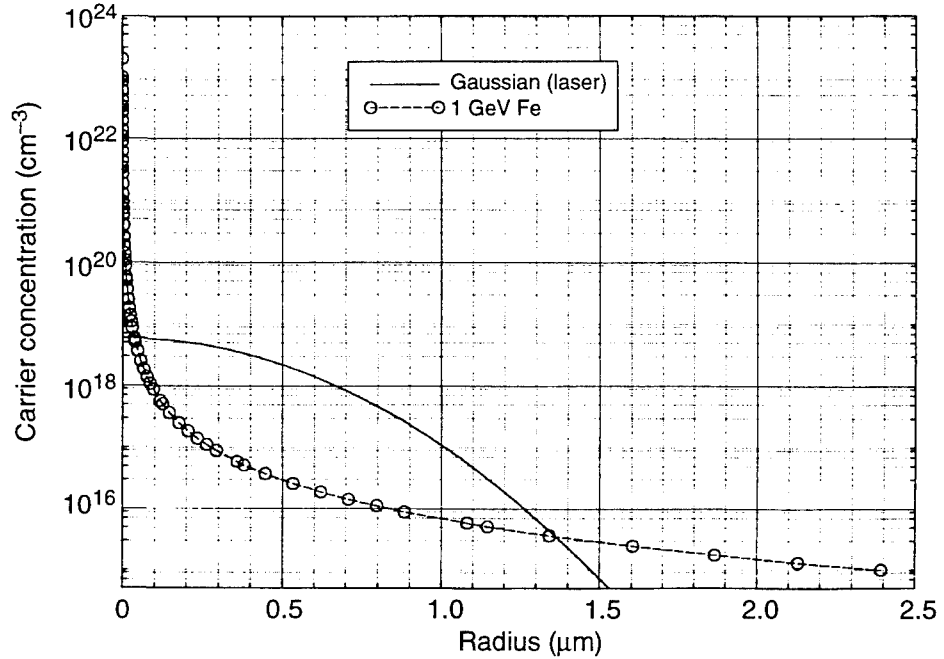
The light is focused with a lens to a small spot with a diffraction-limited diameter that depends on the wavelength of the light. The resulting charge track will be considerably wider than the track produced by a low-energy accelerator ion, but not that much different from a high-energy cosmic ray ion. However, the charge distribution will be very different. Figure 1 compares the lateral charge track profile generated by a 1-GeV Fe ion (calculated using TRKRAD) and a Gaussian laser beam with the same incident LET. Although the two tracks have comparable widths, their profiles differ significantly. Therefore, effects that depend on charge density will result in different amounts of charge being collected for the two cases.

The diameter ( $\omega_0$ ) of the diffraction-limited spot is given by

$$\omega_0 = \frac{4 \cdot f \cdot \lambda}{\pi D} \quad (1)$$

where  $f$  is the focal length of the lens,  $\lambda$  is the wavelength of light, and  $D$  is the diameter of the lens. For most of our experiments we used a  $40\times$  lens with a working distance of 3 mm and a diameter of 4 mm, giving a focused spot with a diameter of 1.0 and  $0.8 \text{ }\mu\text{m}$  for light with wavelengths of 1000 and 800 nm, respectively. This is comparable to the diameter of the high-energy ion-generated charge track. If the incident beam diameter is larger than the diameter of the objective lens, the beam is diffracted and forms a

Figure 1. Radial charge density profile for 1-GeV Fe ion and pulsed laser beam at distance of 0.125 m below surface. Incident LET ion and laser beam are the same.



series of Newton rings at the focus rather than a smooth Gaussian profile. By ensuring that the beam diameter is smaller than the lens diameter, Newton rings can be minimized. However, Newton rings should not significantly affect measurements of relative upset thresholds.

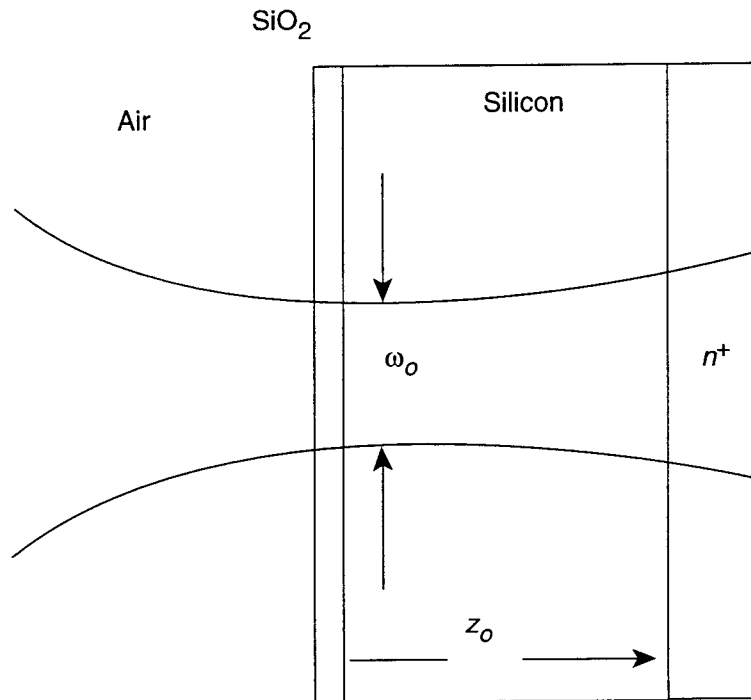
The above calculation is for the size of the spot on the surface of the semiconductor. It should be pointed out that every lens has a depth of field given by the confocal length, which is the distance in front of and behind the focus at which the cross-sectional area doubles in size. The confocal length,  $z$ , is given by

$$z = \pi \eta \frac{\omega_o^2}{\lambda} \quad (2)$$

where  $\omega_o$  is the minimum diameter,  $\lambda$  is the wavelength of light, and  $\eta$  is the index of refraction for silicon ( $\eta = 3.0$ ). Using formula 2, the confocal length in silicon for our lens is calculated to be about 7  $\mu\text{m}$  for light with a wavelength of 0.8  $\mu\text{m}$ . Thus, at a depth of 7  $\mu\text{m}$ , the diameter of the beam has increased by a factor of 1.41 and the charge density has decreased by a factor of 2, neglecting absorption.

Figure 2 shows the longitudinal profile of the focused laser beam, as well as the confocal length and the diameter of the focus spot. The light does not form a cone with an infinitely sharp point at the focus. As can be seen from the figure, the wavefront at the focus is parallel to the semiconductor surface and the wavevector is normal to the surface. One can still use Snell's law to calculate the divergence of the beam in the far field. For the objective lens we used, the maximum angle to the normal in the far field region is 34°, resulting in a divergence angle of 10° in the silicon. Both absorption and spreading of the beam lead to a reduction of the charge density with distance below the surface. The lower charge density in the laser

Figure 2. Shape of focused laser beam passing from air to  $\text{SiO}_2$  and then Si.  $\omega_0$  is smallest spot size determined by diffraction and  $z_0$  is confocal length, which is length over which beam area doubles in size. Larger index of refraction of Si leads to beam expanding more slowly in Si than in air.



track as compared to the ion track will affect the amount of charge collected because funneling, the shunt effect, and Auger lifetime all depend on charge density. It is not possible to generate charge underneath a metal layer because the large index of refraction of silicon bends the light toward the normal when it enters the silicon.

### 3.3 Funneling

When a charge track with a density greater than the doping density of the semiconductor passes through a junction, the electric field associated with the junction is distorted, producing a "funnel" that gives rise to additional charge collection. The track density determines the length of the funnel which, in turn, determines the amount of extra charge collected. By showing experimentally that the amount of charge collected across a diode junction irradiated with a laser pulse depends on the total beam energy to the  $4/3$  power [11], we confirmed that funneling plays a role in charge collection for both ions and laser light [12]. However, to see the power dependence in devices with high doping levels using the relatively wide laser beam, we had to use very high laser energies to generate sufficient charge to exceed the background charge density. Obviously, in cases where funneling contributes a significant amount of charge to ion-induced upsets, larger equivalent LETs will be needed for the laser. This is one reason why the laser cannot replace the accelerator for determining absolute values for SEE threshold.

### 3.4 Shunt Effect

Another effect modifying charge collection, and observed with ion beams, was the “shunt” effect. If a single ion passes through two junctions in series, e.g.,  $n/p$  and  $p/n$ , the track of charge will connect the two outer  $n$ -regions via a low resistivity path through the  $p$ -region. Current will then flow between the two outer regions, and the sign of the charge collected at a contact will depend on the sign of the voltage. Using special test structures, we were able to show that the pulsed laser could also produce the shunt effect provided sufficiently high laser energies were used to create the charge track [4].

Additional evidence for the existence of the shunt effect produced by the laser was obtained during an investigation of upsets in the SA3300 microprocessor. We found that we could produce upsets in certain registers when the light was focused on an “on” gate. Normally, on gates are not sensitive to SEU. However, we attributed that upset to a shunt produced by the light in which a track of charge was formed that shunted the drain to the substrate through the well [13]. With the substrate at high voltage, holes could flow along the shunt from the substrate to the drain, thereby raising the voltage on the drain and causing an upset.

Thus, two effects (funneling and the shunt) that are known to control charge collection from ion-generated tracks, also play a role in laser-light-generated tracks. However, because both effects depend critically on the charge density, the upset thresholds measured with the laser will typically be greater than those measured with an ion beam.

### 3.5 Carrier Lifetime

After the track is formed, the charges spread out and recombine. As they do so, the funnel collapses, and when the track density drops below that of the background carrier density, the funnel disappears. Many factors influence the carrier lifetime, but at high carrier densities, Auger recombination dominates. Auger recombination occurs when free electrons in the track collide, resulting in one electron losing energy to another.

The Auger recombination time depends on carrier density as:

$$\tau = \left( \frac{3n_i^2}{\Delta n^2} \right) \tau_i \quad (3)$$

where  $n_i$  is the intrinsic carrier concentration,  $\Delta n$  is the injected carrier density, and  $\tau_i = 4.48 \times 10^9$  s is the intrinsic Auger lifetime.

At high densities the recombination time becomes very short, limiting the amount of collected charge. In fact, the lifetime is on the order of a picosecond when the carrier density approaches  $10^{21}/\text{cm}^3$ . Results from PADRE, a three-dimensional computer code for calculating device response to disturbances such as charge injected by heavy ions, show that less than 100

percent of the injected charge is actually collected, and that the discrepancy is largely due to Auger recombination [14]. This effect is more pronounced for heavy ions that produce denser tracks.

The Auger recombination time is much shorter in an ion-generated charge track than in the much lower density track produced by laser light. Thus, more charge is lost via Auger recombination in the ion track than in the laser-light charge track. Charge lost via Auger recombination has been observed experimentally for heavy ion fission products in surface barrier detectors [15]. Another study shows that the amount of charge in the track lost to recombination depends on the carrier lifetime relative to the plasma erosion time,

$$\frac{\delta n}{n} = \frac{t_p}{t_r} \quad (4)$$

where  $t_p$  is the plasma lifetime and  $t_r$  is the recombination time [16]. Furthermore, the plasma lifetime decreases with increasing field [17]. These effects are most easily studied with computer modeling because of the difficulty of including all the effects in an analytic expression.

Recombination and funneling tend, to a certain degree, to cancel each other out. Thus, the differences in the amount of charge collected by ions and laser light arising from differences in track charge density are reduced, and the threshold LETs measured by the two techniques, in some cases, may not be significantly different. In fact, in a recent publication Gossett and Johnston show, using PISCES calculations, that, for lightly doped materials, the differences in charge collection between tracks from ions and laser light are small [18]. The differences become more significant for more highly doped materials.

### 3.6 Diffusion

High-energy cosmic rays pass right through a circuit, producing very long charge tracks. Charge generated within a diffusion length of a junction in a bulk device will also be collected, supplementing the charge collected by drift. Therefore, for accurate accelerator testing, it is necessary to choose ions that have sufficient energy to penetrate to a distance beyond the junction comparable to the diffusion length. Using laser light to generate charge tracks that penetrate beyond the junction is a simple matter of selecting the right wavelength. In the case of silicon devices, the 1.06- $\mu\text{m}$  output of a Nd:YAG laser has a penetration depth of a few hundred microns, well beyond typical junction depths.

As pointed out earlier, most devices are currently made in epitaxial silicon layers deposited on highly doped substrates. Charge collection from highly doped substrates is significantly reduced because the diffusion length  $L$  is proportional to  $(\mu\tau)^{0.5}$ , where  $\mu$  is the mobility and  $\tau$  is the lifetime. At a density of  $>10^{19}/\text{cm}^3$ ,  $\mu$  is reduced by a factor of about 5 and  $\tau$  is reduced by a factor of more than 100, so that the total charge collected by

diffusion from the highly doped substrate is reduced by more than an order of magnitude and can be neglected. Therefore, only charge generated in the epitaxial region need be considered.

### 3.7 Generation Time

Another difference between ions and laser light is the time it takes to generate the charge track. In the case of the ion, the track is generated in less than a picosecond. On the other hand, the time for the charge to be generated with the laser light is determined by the length of the laser pulse. The laser we used for our experiments had a pulse length of 30 ps. There are lasers currently available with pulse lengths in the femtosecond range that should more closely match the generation time for the ion. However, it is not necessary to go to such short pulse lengths. As long as the pulse length is shorter than the response time of the circuit, one can ignore the differences between the charge generation times for ions and laser light. It is worth noting that very short laser pulses result in higher laser intensities, which, as pointed out later in this report, lead to nonlinear effects. For devices currently in use, it is the total integrated charge that is the relevant factor determining upsets, and the actual time evolution is not important. This was confirmed by charge-collection measurements made on test structures with heavy ions, which showed rise times typically on the order of 50 to 100 ps, and decay times of a few hundred picoseconds [19]. Charge-collection times for fast devices, such as GaAs-based structures, will be much shorter, and it may be necessary to use a laser with a shorter pulse length.

### 3.8 Reflections

The amount of light contributing to charge generation will be determined by reflections off the front surface of the semiconductor. For a bare silicon surface and at low light intensities, the reflection  $R$  for normal incidence is given by

$$R = \left| \frac{\eta - 1}{\eta + 1} \right|^2 \quad (5)$$

where  $\eta$  is the wavelength-dependent index of refraction of silicon; it has been tabulated in the literature [20]. As pointed out in section 3.2, it is not necessary to consider light that is not normal to the surface, and equation (5) is suitable for calculating the total amount of light reflected.

If the Si surface is covered with a dielectric, the reflection will depend on the index of refraction of the dielectric, as well as its thickness. If the index of refraction of the dielectric equals the square root of that of Si, depending on the thickness, the dielectric can act either as an antireflection coating, permitting all the light to enter the semiconductor, or alternatively, as a reflecting coating, permitting very little light to enter the semiconductor. We have calculated the maximum and minimum amount of light reflected

from a Si surface covered with  $\text{SiO}_2$  and found that the variation in reflectivity as a function of  $\text{SiO}_2$  thickness is no more than 5 percent. This has important ramifications for hardness assurance because any variations in the amount of charge needed to upset different cells should be due to variations in SEE immunity rather than variations in the amount of light reflected from a Si surface covered with a layer of  $\text{SiO}_2$  whose thickness can vary because of poor process control during manufacture.

Reflections from the back surface that may contribute to multiple upsets or add to the amount of charge generated in a particular junction should typically be of no concern because the light is diverging and the back surface is usually rough. Both of these factors contribute to the reduction of the light intensity by orders of magnitude by the time it again reaches junctions near the front surface.

### 3.9 Cross-Section

The SEU cross-section is obtained from ion data by counting the number of upsets per unit fluence at high LETs. The pulsed laser does not give SEU cross-sections directly because the beam probes only a very localized area, and because parts of the sensitive regions are covered with metal, which prevents the light from reaching the silicon. There is, however, an indirect way of measuring the asymptotic cross-section with the laser by first determining which transistors are sensitive and then multiplying their sensitive areas by the total number of such transistors. This has been done for an analog circuit, and the cross-section obtained from ion-beam experiments ( $7 \times 10^{-4} \text{ cm}^2$ ) agreed remarkably well with that obtained using the technique described above ( $6 \times 10^{-4} \text{ cm}^2$ ) [21]. Care should be taken to include all the sensitive areas in trying to determine total SEU cross-section. For instance, when testing an SRAM, one should include not only the memory cells, but also the control circuitry around the edge of the chip.

### 3.10 Nonlinear Effects

High laser-light intensities used for testing circuits with high LET upset thresholds lead to additional absorption mechanisms that modify the relationship between light intensity and carrier density. In addition, highly doped regions in the semiconductor modify the amount of charge generated by the light. Consequently, if one wishes to calculate the LET for laser light, one must consider the contributions to the absorption by these other mechanisms. Nonlinear effects must also be considered for hardness assurance measurements. For example, if the doping of an  $n$ -well in a silicon transistor is increased, the  $n$ -well may be only slightly affected because neither the junction capacitance nor the resistance will change, but the amount of charge generated by the laser light will be altered, particularly if light with photon energy close to the bandgap of silicon is used. We will discuss briefly the role played by nonlinear effects.

Some of the possible mechanisms that may lead to nonlinear effects are [22]

- two-photon absorption,
- free-carrier absorption,
- bandgap narrowing, and
- lattice heating.

### 3.10.1 Two-Photon Absorption

Absorption by both one- and two-photon processes is governed by the following equation:

$$I = I_0 \frac{e^{-\alpha x}}{1 + \left(\beta \frac{I_0}{\alpha}\right)(1 - e^{-\alpha x})} \quad (6)$$

where  $I$  is the intensity of the light,  $\alpha$  is the linear absorption coefficient and  $\beta$  is the nonlinear two-photon absorption coefficient. At a wavelength of 1.06  $\mu\text{m}$ , the value of  $\alpha$  for Si is 10  $\text{cm}^{-1}$  and  $\beta = 30 \text{ cm/GW}$ . For an LET of 10  $\text{MeV-cm}^2/\text{mg}$  and a pulse length of 30 ps,  $I_0$  is 0.075  $\text{GW/cm}^2$ . Nonlinear absorption has a magnitude of about 1 percent of the linear absorption, and can be ignored. At higher LETs the differences become more pronounced, approaching 25 percent at an LET of 100  $\text{MeV-cm}^2/\text{mg}$ . Clearly, any calculation of equivalent LET for laser light must, at high energies, take nonlinear effects into account. By using equation (4), the effects of two-photon absorption can be included in the calculation of LET.

However, as pointed out previously, it is not necessary to use light with a wavelength of 1.06  $\mu\text{m}$  because, in most devices, the light only needs to generate charge near the surface. By selecting a wavelength of 850 nm,  $\alpha$  increases to 400  $\text{cm}^{-1}$ , whereas  $\mu$  barely changes, so that the nonlinear contribution ( $\beta/\alpha$ ) is reduced by a factor of 40 and can be ignored.

### 3.10.2 Free-Carrier Absorption

Light can also be absorbed by free carriers in highly doped regions. The effect only becomes important when the plasma frequency is comparable to or greater than the frequency of the light ( $10^{15} \text{ s}^{-1}$ ). Using the formula for the plasma frequency,

$$\omega_p^2 = \frac{Ne^2}{m^* \epsilon_0 \epsilon_r} \quad (7)$$

where  $N$  is the carrier density,  $m^*$  is the carrier effective mass,  $e$  is the electron charge,  $\epsilon_0$  is the permittivity, and  $\epsilon_r$  is the dielectric constant, one obtains a plasma frequency of  $10^{14} \text{ s}^{-1}$  (for a carrier density of  $10^{19}/\text{cm}^3$ ), which is much less than the frequency of light [23]. Free-carrier absorption

is negligible and can be ignored. One must have carrier densities at least two orders of magnitude greater to experience any appreciable free-carrier absorption.

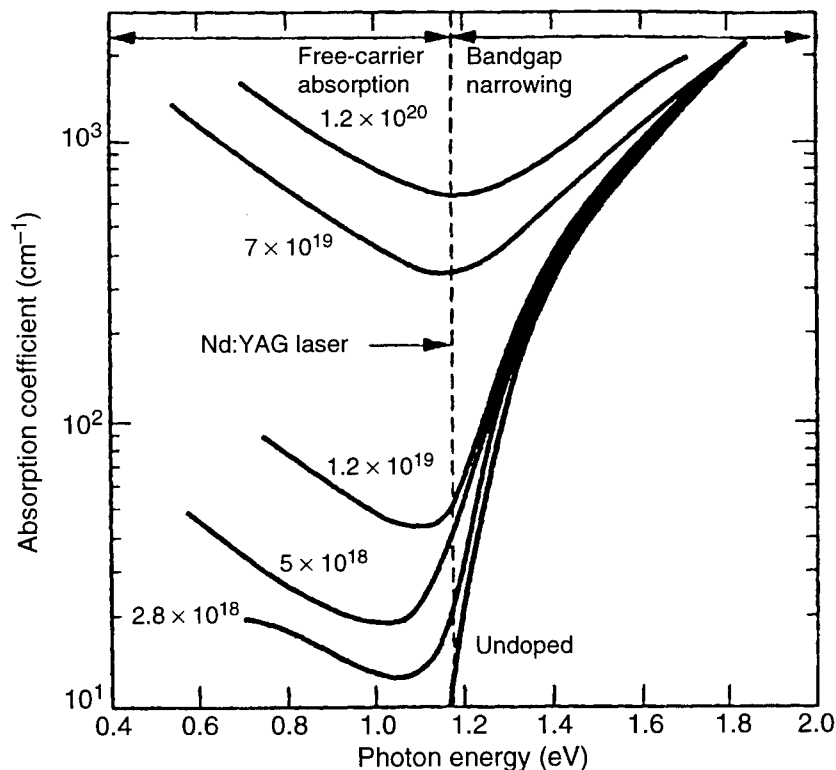
The same analysis applies to absorption by carriers generated by the laser light, i.e., the leading edge of the laser pulse generates carriers that can absorb light from the trailing edge of the pulse. We find that there is negligible free-carrier absorption for light up to incident equivalent LETs well above  $100 \text{ MeV-cm}^2/\text{mg}$ , particularly if light with a wavelength of 850 nm is selected.

### 3.10.3 Bandgap Narrowing

The energy bandgap depends on the carrier density through two effects—bandgap renormalization and the Burstein-Mott shift. High doping levels reduce the bandgap through bandgap renormalization, whereas the Burstein-Mott shift increases the effective bandgap because carriers at the bottom of the conduction band in *n*-type material fill up states that are then not available for electron transitions from the valence band. In silicon, the net effect of bandgap renormalization and the Burstein-Mott shift is to reduce the bandgap and, thus, increase the absorption as the carrier density increases.

Figure 3 shows the effects of both bandgap narrowing and free-carrier absorption [24]. By selecting a wavelength of 850 nm, one can see from the figure that the absorption coefficient does not change with carrier density.

Figure 3. Absorption coefficient for Si as function of photon energy, taking both free carrier absorption and bandgap narrowing into account. [From A. H. Johnson, IEEE Trans. Nucl. Sci. NS-40, 1694 (1993).]



This is another reason why, for most devices, it is better to use light with a wavelength of 850 nm.

### 3.10.4 Lattice Heating

Some fraction of the absorbed light will be converted to heat, leading to an increase in the lattice temperature and a change in the energy gap of the semiconductor. In fact, as the temperature increases, the bandgaps of both Si and GaAs get smaller, resulting in an increase in the absorption. An analysis of this problem would require considerable effort. However, we have found experimentally that Si melts only when more than two orders of magnitude more energy is deposited in the material than what we used to upset the most immune circuits ( $\text{LET} = 120 \text{ MeV-cm}^2/\text{mg}$ ), which we tested with  $1.06\text{-}\mu\text{m}$  light. Consequently, lattice heating effects can safely be neglected.

### 3.11 Calculation of Laser LET

In this section we outline the calculation for converting laser energy absorbed to LET for comparison with ions. The calculation assumes that the linear energy density of charge created by the laser light and the ion beam are equal, that the absorption coefficient is a constant with distance into the semiconductor, and that nonlinear effects can be neglected. For strongly absorbed light, the calculation must be modified and the intensity of the light must be integrated over the appropriate distance to obtain the total amount of charge deposited.

Assume that the pulse of light has energy  $J$  (Joules) where  $1 \text{ MeV} = 1.6 \times 10^{-13} \text{ J}$ . If  $R$  is the fraction of light reflected from the surface of the chip, then the amount of energy entering the silicon is

$$E_o = \frac{(1 - R)J}{1.6 \times 10^{-19}} \text{ MeV} . \quad (8)$$

According to Beer's Law, the intensity of light  $I(x)$  in an absorbing medium decreases exponentially with distance ( $x$ ) from the surface ( $x = 0$ ) according to

$$I(x) = I_o e^{-\alpha x} . \quad (9)$$

Assuming a small absorption constant, the change in intensity near the surface is given by

$$I_o - I = I_o - I_o e^{-\alpha x} = I_o (1 - 1 + \alpha x) = I_o \alpha x . \quad (10)$$

Therefore, since  $I_o$  is proportional to  $E_o$ , substituting  $E_o$  from equation (8) for  $I_o$  in equation (10), we obtain

$$\frac{dE}{dx} = \frac{(1 - R)J\alpha}{1.6 \times 10^{-13}} . \quad (11)$$

Now,  $N_L$  is the linear density of  $e-h$  pairs by the laser and is given by

$$N_L = \frac{(1-R)J\alpha}{1.6 \times 10^{-13} E_{Si}} \quad (12)$$

where  $E_{Si}$  is the photon energy required to generate one  $e-h$  pair. For an ion of energy  $E$  impinging on a material of density  $r$ , the LET is given by

$$LET = \frac{1}{\rho} \frac{dE}{dx} . \quad (13)$$

Therefore,

$$\frac{dE}{dx} = \rho LET . \quad (14)$$

$N_{ion}$ , the number of  $e-h$  pairs produced per unit length, is given by

$$N_{ion} = \frac{1}{E_{ion}} \frac{dE}{dx} = \frac{\rho}{E_{ion}} LET \quad (15)$$

where  $E_{ion} = 3.6$  eV.

By equating  $N_{ion}$  with  $N_L$ , we obtain

$$\frac{\rho LET}{E_{ion}} = \frac{(1-R)\alpha J}{1.6 \times 10^{-13} E_{Si}} \quad (16)$$

and finally

$$LET = \frac{(1-R)\alpha J E_{ion}}{\rho 1.6 \times 10^{-13} E_{Si}} . \quad (17)$$

If the values listed in table 1 are used for Si, one can express the LET as

$$LET = 0.0527 J (\text{MeV-cm}^2/\text{mg}) \quad (18)$$

where  $J$  is in picojoules.

At higher photon energies where the absorption is much larger, the intensity changes rapidly with distance and an integral form of the equation must be used. Modifying the equation is simple and the details will not be presented here.

**Table 1. Values used in calculation of LET.**

Symbol	Value
$E_{ion}$	3.6 eV
$E_{Si}$	1.1 eV
$\alpha$	$10 \text{ cm}^{-1}$
$\rho$	$2330 \text{ mg/cm}^3$
$R$	0

## 4. Equipment and Procedure

In this section we describe how measurements of SEE sensitivity are carried out and what equipment is necessary for doing the measurements. We also include a discussion on what measurements can be automated.

### 4.1 Equipment

Figure 4 shows the layout of the system used to test circuits for SEEs. Table 2 lists the components necessary for SEE testing with a pulsed laser, suggested manufacturers, and their approximate costs. There are alternatives to the manufacturers and they can be found in optics trade journals such as *Laser Focus World*.

Figure 4. Schematic of equipment needed for pulsed laser SEE testing.

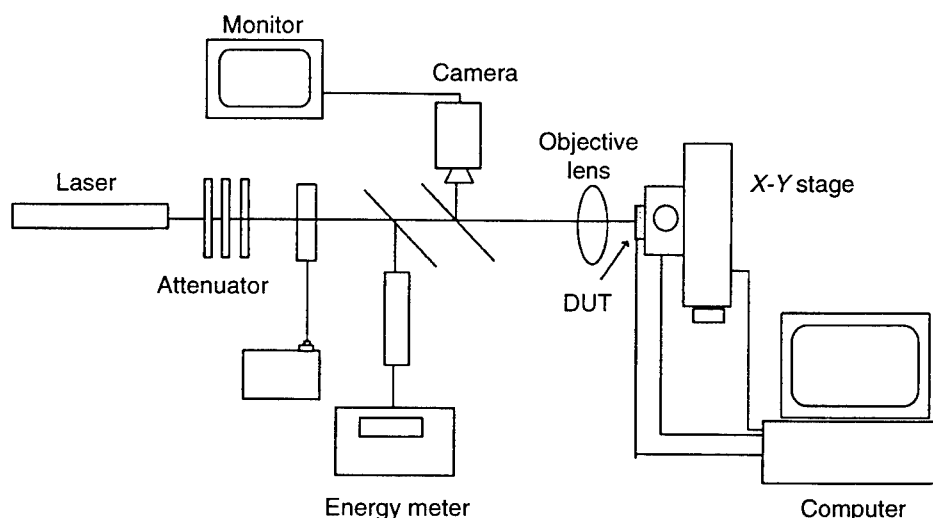


Table 2. List of equipment needed for SEE testing.

Equipment	Manufacturer	Cost (\$K)
Optical table	Newport	10
Pulsed Nd:YAG (30 ps)	Continuum	65
Dye laser (for testing GaAs)	Continuum	25
Ar ion-pumped Ti:sapphire laser	Coherent	127.5
X-Y stage	Aerotech	15
Energy meter and probe	Laser Precision	5
Electronic shutter	Melles Griot	0.5
Charge-coupled device camera	Pulnix	1
Black and white monitor	Sony	0.55
Achromatic microscopic objective lens (80 $\times$ , NA = 0.75)	Olympus	5.8
Mirrors	Newport	0.1
Neutral density filters (set)	Newport	0.9
Half-wave plate	Special Optics	0.5
Polarizers (2)	Special Optics	1
Computer	Any brand	2
Stands/holders	Newport	1

Table 2 shows that the entire test setup can be purchased for around \$135K including the dye laser and about \$170K if the Ti:sapphire laser is used. Although this is a sizeable investment, there is very little cost involved in running and maintaining the system other than personnel costs. Tests are very simple to run and the only extensive training needed is for maintaining the laser.

**Vibration-isolation table.** The entire pulsed laser system, apart from the laser power supply, should be mounted on a vibration-isolated optical table because the slightest movement of the chip with respect to the beam can alter the value of the upset energy being measured. A table with dimensions 8 by 6 ft and supported by air-filled shock absorbers provides sufficient space and isolation for the laser, optics, and stages. By securely mounting everything to the table, one can minimize the effects of vibration.

**Pulsed laser.** A source of pulsed laser light is necessary for producing upsets. Laser specifications for doing SEE testing include

- pulse length significantly shorter than the response time of the circuit,
- photon energy larger than the semiconductor bandgap, and
- pulse energy sufficient to produce upsets in hardened devices.

There are two laser systems available for doing SEE testing that meet the above requirements:

- pulsed picosecond dye laser pumped with a Nd:YAG laser, and
- Ti:sapphire laser pumped with an argon laser.

(All our work was done with the Nd:YAG pumped dye laser or just the Nd:YAG laser by itself.) Both laser systems provide tunable sources of light, although their operations are quite different. The Ti:sapphire laser is by far the simpler system to use because one does not have to bother with regular changing of dyes—a messy and time-consuming task. As previously pointed out, testing epilayer Si devices should be done with light with a wavelength of 850 nm to minimize non-linear effects arising from two-photon absorption, bandgap renormalization, and free-carrier absorption. An additional advantage of using light at that wavelength is a smaller spot size.

The Nd:YAG/dye laser operates at 10 Hz with pulse lengths of 30 ps, whereas the Ti:sapphire operates in the megahertz range and can supply pulses down to femtoseconds in length. Both types of lasers have sufficient energy per pulse to produce upsets in circuits that will upset when exposed to cosmic ray ions. For most measurements, neutral density filters are required to attenuate the beam energy to values close to upset threshold.

The beam exiting the dye laser diverges relatively rapidly so that either a collimator must be used to produce a non-diverging beam of light, or the device to be tested must be located as close as possible to the dye laser

beam exit. This is because a beam with a diameter larger than the aperture of the focusing lens will be degraded by the lens, resulting in interference fringes on the circuit being tested. The interference pattern consists of an Airy disk and rings. Whether these have much effect on the amount of charge collected and, thus, on the measured upset threshold has not yet been established.

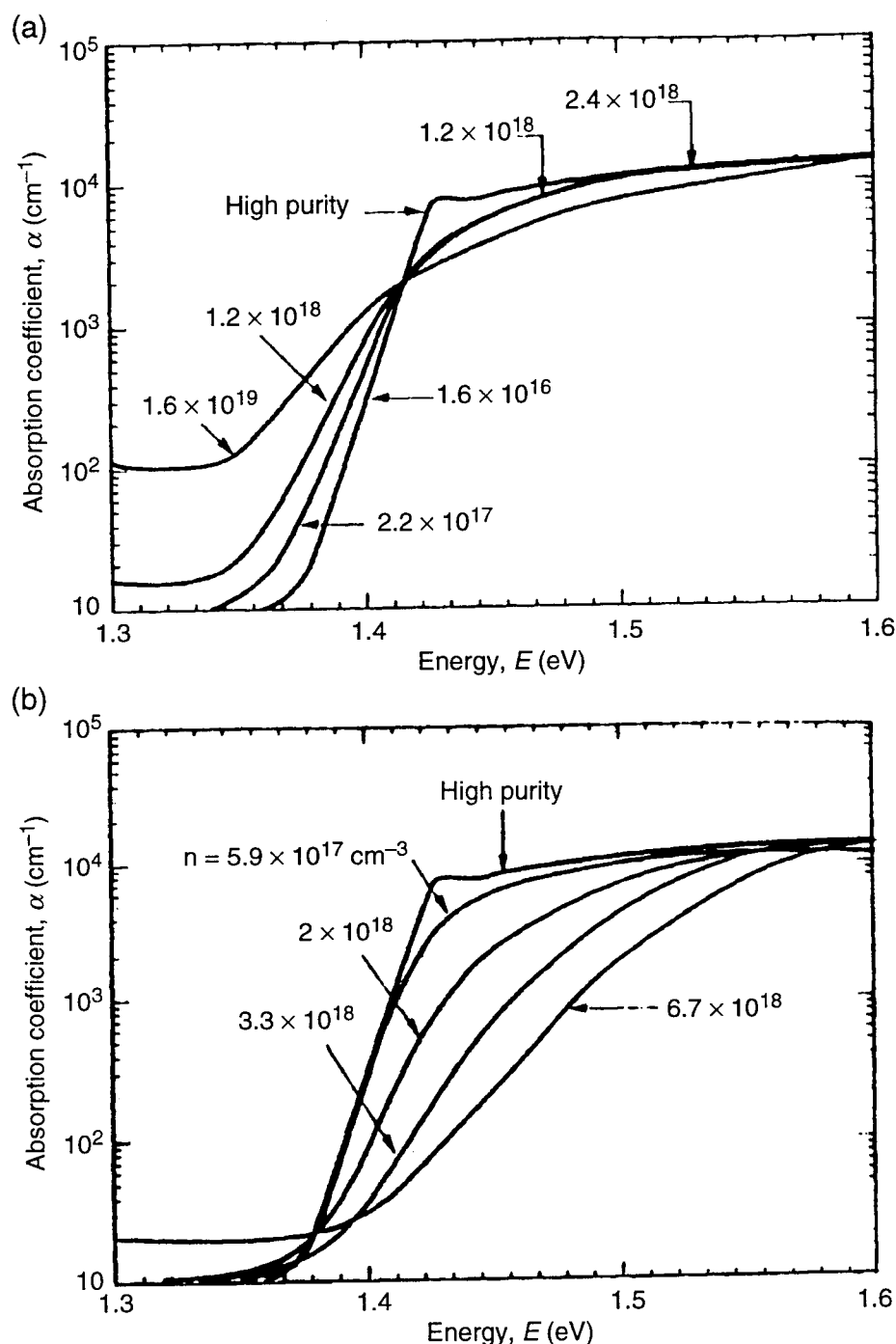
The Nd:YAG/dye laser fires at a rate of 10 Hz, which is convenient for doing upset measurements. It can also be run in the single shot mode, but the pulse energy varies widely, making it difficult to measure exact upset thresholds. We have found that the most convenient way of doing the measurements is to let the laser run at 10 Hz and use an electronic shutter controlled either by hand or by a computer and set to a shutter speed of 1/15 s to allow only a single pulse through at any time. The circuit can then be monitored by the operator or computer to determine whether an upset has occurred. If an aperture is not used, the laser pulses striking the circuit at a rate of 10 Hz arrive at a rate too fast for an operator to manually adjust the system and record the data. In that case, a computer will be required to determine upset, measure the energy, and reset the system.

The argon/Ti:sapphire laser can be run in the kilohertz range, which requires a fast circuit tester to test for upsets. Current memory testers can easily test at this rate.

When using the Nd:YAG laser for SEE testing, one must take care to ensure that the measurements are not affected by two factors associated with the laser. The first is the emission of RF noise by the electronics that control the firing of the laser. A high-voltage pulse is used to trigger the Pockel cell and, if proper care is not exercised, the associated RF noise can be picked up by cables connecting the chip to the test equipment and induce upsets by adding to the amount of charge collected. Two solutions to this problem are shielding and separating the circuit being tested from the laser by a large distance, on the order of 25 ft. Shielding has proven effective in some of our experiments. Strategies include shielding the cables, using twisted cables, using push-pull control lines and, in an extreme case, constructing a Faraday cage and isolating the circuit and all the test equipment. The second solution means that all the equipment cannot be mounted on a single isolation table, so vibrations may become a problem. Also, a beam collimator will be needed to maintain the beam diameter over the long distance. The second problem with the laser is that if the voltage to the flashlamps is not properly adjusted, double pulses, separated by microseconds, may be emitted. The double pulses have, in the past, caused confusion. When testing an SRAM, we found that, at energies considerably above the threshold, the circuit would not upset, and we attributed it to the fact that the first pulse produced an upset, and the second pulse switched the circuit back to its original state, with the result that no upset was observed.

The Nd:YAG/dye laser system can also be used to test GaAs circuits because the photon energy can be tuned to values close to the bandgap energy of GaAs. Figure 5 shows the absorption as a function of wavelength

Figure 5. Energy dependence of absorption coefficients for both (a) *n*- and (b) *p*-type GaAs as function of doping.



for both *n*- and *p*-GaAs [25]. In the vicinity of the bandgap energy of GaAs, the absorption is a strong function of carrier density due to bandgap renormalization, free carrier absorption, and the Burstein-Mott shift. If a photon energy of 1.6 eV is selected, the penetration depth is about 1  $\mu\text{m}$ , which has proved to be suitable for metal-semiconductor field-effect transistor (MESFET), modulation-doped FET (MODFET) and heterojunction bipolar FET (HBT) technology, where all the action occurs near the surface. Of the two types of lasers, Ti:sapphire is more attractive because maintaining and aligning the dye laser is a more tedious and time-consuming procedure.

It should be pointed out that semiconductor bandgaps are sensitive to temperature, generally decreasing with increasing temperature. We have found that some GaAs circuits run very hot, and by selecting wavelengths where the photons have much larger energies than the bandgap energy, changes in temperature will not affect absorption.

**X-Y stage.** For testing, the circuit is moved until the sensitive node is positioned in the beam. An X-Y stage with 0.1- $\mu\text{m}$  step size is necessary for accurate positioning of the circuit in the beam. This is particularly important when the dimensions of the sensitive areas are close to the diameter of the beam, because, if the step size is too large, it will be extremely difficult to position the beam optimally. By connecting a computer to the stage controller, it is possible to generate contour plots of upset sensitivity versus position. It is essential that there be very little backlash in the X and Y stages when doing contour plots.

**Energy meter.** The energy needed to produce an upset is measured with an uncalibrated energy probe and meter. A beam splitter in the form of a thin piece of glass is set in the beam at a 45° angle, and about 5 percent of every pulse is directed at the probe. In this way, the energy of each pulse is known to within a calibration factor that is determined either before or after the measurement. The calibration factor is calculated by placing a calibrated probe in the beam where the chip would be and comparing the absolute value measured with the calibrated probe to that measured by the noncalibrated probe. The energy meter has an RS232 connection for transferring the energy readings to a computer. Clearly, the computer can be used to simplify data acquisition by automating the system. This will be described in more detail later.

**Electronic shutter.** For reliable measurements, we used an electronic shutter set to 1/15 s to allow only a single pulse to reach the circuit being tested. Since the shutter was electronically controlled with transistor-transistor logic (TTL) devices, it could also be computer controlled. As pointed out previously, we have found that running the laser at 10 Hz and using a shutter to allow only one pulse at a time to reach the circuit gives better results because the pulse energy does not vary widely when the laser is run at 10 Hz. This makes it possible to do rapid and accurate measurements of upset threshold.

**Attenuator.** Measurements of SEE threshold are done by exposing the sensitive area on the circuit to a low-energy beam and increasing the energy until upsets are registered. The LET can then be calculated knowing the absorption coefficient of the light and the energy in the pulse. Thus, the LET can be changed by varying the wavelength or intensity of the light. In most experiments, the wavelength is fixed by the requirement that the light should have a penetration depth much larger than the junction depths. Thus, to change the LET, the beam energy is changed. We have tried various techniques to control the pulse energy, including a wheel with an exponentially varying optical density around the circumference and discrete neutral density filters. However, both these schemes proved

unsatisfactory because rotating the wheel or changing the number of neutral density filters caused a slight movement of the beam relative to the chip. The most effective technique that did not move the beam involved the use of a half-wave plate sandwiched between two polarizers. Rotating the half-wave plate to vary the transmitted intensity caused no shift in the beam. In an automated system, a motor could be used to rotate the half-wave plate.

*Charge-coupled device (CCD) camera and monitor.* In order to position the laser on the SEE-sensitive area of the circuit, it is necessary to be able to view the circuit and laser beam simultaneously. In our system we used part of a microscope housing that contains all the components necessary for illuminating and viewing the circuit, as well as for focusing the beam on the circuit. The laser light is directed along the axis of the microscope housing, at the end of which is an objective lens for focusing the light. Attached to the housing are a lamp and an eyepiece. The light from the lamp is directed onto the circuit by means of a beam splitter situated along the axis of the microscope housing. Another beam splitter directs the light reflected from the circuit into the eyepiece for viewing. It is not absolutely necessary to use a microscope housing. The same setup can be achieved with beam splitters and lenses, as indicated schematically in the layout of the equipment. A problem with the illuminator does arise when testing DRAMs that are extremely sensitive to light. Some DRAMs are so sensitive that even room lights will cause them to upset. In that case, the illuminator must be turned off when doing the measurement. Periodically, the light should be turned back on to check for proper focus.

A CCD camera was positioned at the eyepiece because the high energy in each laser pulse makes it extremely dangerous to look directly into the eyepiece. The CCD camera is attached to a monitor that displays the circuit and the laser spot focused on the circuit. If a picture is needed of the area of the circuit being tested, a frame grabbing program can be used that will show, for every measurement made, the location of the laser beam on the circuit. When testing sensitive DRAMs, so little light is needed to produce an upset that the beam is not visible on the monitor. In addition, the illuminator must be turned off because its light can also produce upsets. Under those circumstances, one is working most of the time in the dark, and the illuminator must occasionally be turned on and the light intensity increased so that its image becomes visible on the monitor to ensure that the beam is still in focus.

*Objective lens.* The laser light is focused by an objective lens onto the circuit. The diffraction-limited size of the beam, given by equation (1), shows that, to obtain a small spot size, one needs a beam with a small  $f$  number ( $f/D$ ) and a small wavelength. The wavelength is, to a large extent, fixed by the semiconductor properties, so the only parameter left to select is the  $f$  number of the lens. For instance, in our case, when using the 1.06- $\mu\text{m}$  laser light, and a lens with an  $f$  number of 0.75 (magnification of 40 $\times$  and a working distance of 3 mm) the minimum spot size is 1.0  $\mu\text{m}$ . For light with a wavelength of 850 nm, the spot size would be only 0.85  $\mu\text{m}$  in diameter. It

is very difficult to make lenses with high magnification that have smaller  $f$  numbers. When using 1.06- $\mu\text{m}$  wavelength light, one must consider the problem of chromatic aberration, where light with different wavelengths has different focal lengths. Chromatic aberration results in either the circuit or the laser light being in focus, but not both at the same time.

The usual solution is to use achromatic objective lenses that compensate for the wavelength-dependence of the focal length, and the lens listed in table 2 and manufactured by Olympus is one possibility. The high cost of that lens is due to the fact that most achromatic lenses work only over a limited range and do not cover the visible and IR portions of the spectrum simultaneously. Another alternative is to use reflecting instead of refracting optics. A Cassegrain-type reflecting mirror system, consisting of a large concave mirror with a hole in the middle, through which the laser light passes before being reflected off a convex mirror back onto the concave mirror, can be used to focus the light. However, the system proved unsatisfactory because the quality of the image was poor and light leaked around the small mirror, making it a problem to obtain small spot sizes.

Since we did not know about the achromatic lens from Olympus, we were forced to use a technique that involved focusing the beam on some flat metal portion of the circuit and marking the spot on the monitor's surface with ink. Then, we refocused and moved the circuit until the ink spot was located on the region we wished to test. We then refocused the laser spot and measured the upset levels. At 850 nm, one can use a normal microscopic objective lens because the Si CCD camera will image both the circuit and the light spot with little distortion due to achromaticity, especially if a low-bandpass filter is used in front of the camera that transmits light with a wavelength longer than 800 nm. This is ideal for our applications, because SEE laser testing requires viewing the circuit and the laser light simultaneously so that the light spot can be accurately positioned.

**Magnification.** The total magnification achieved is the product of the magnifications of the objective and eyepiece lenses. We typically used a 40 $\times$  objective lens and a 20 $\times$  eyepiece lens for a total of 800 $\times$ . In some cases, we used a 150 $\times$  objective lens and a 20 $\times$  eyepiece lens, which gave a total magnification of 3000 $\times$ .

**Automatic focus system.** To correct for any movements of the chip with respect to the objective lens, one should use an automatic focus system. This is especially critical when using a lens with a very short working distance, because the slightest movement of the chip with respect to the objective lens results in a defocused image. Sockets for chips are frequently mounted on flexible boards with heavy cables attached. The slightest change in tension will result in the image of the circuit becoming defocused. Our system does not yet contain an automatic focusing feature, forcing us to rely on manual focusing when the image on the screen begins to become fuzzy. We are not sure how well an automatic system would work, considering that high-magnification objective lenses have a smaller depth of field than the distances between valleys and peaks, characteristic of the circuit topology.

*Sockets.* Finally, the sockets themselves may inhibit SEE laser testing because they are so constructed as to prevent the objective lens from being positioned close to the chip surface. Modifications to the sockets are then necessary.

## 4.2 Test Procedure

Before testing a circuit for SEE, one must be familiar with the function and layout of the chip. For example, in the case of SRAMs, the sensitive areas are the drains of the four transistors (two cross-coupled inverters). It is important to know where the drains are located, their size, and whether or not they are covered with metal. Although tests can be done without detailed knowledge of the circuit layout, having the necessary information has proven to be most useful.

The test equipment necessary for conducting laser SEE testing should be capable of exercising the device under test (DUT). For an SRAM, this is done by having the test equipment write a pattern to the chip and then read the pattern, comparing the new pattern to the old one. If the new pattern differs from the old one, an upset has occurred. The program must be able to identify the location of the upset and then be able to scan only the particular cell being irradiated with the laser light. An additional feature necessary for SEE testing is a latchup monitor that signals a sudden increase in either standby or active current. Tests for multiple upsets should also be included in the software for the electronic tester.

The method for doing SEE measurements is outlined below:

- (1) The chip is delidded and mounted securely in a socket attached to the X-Y stage.
- (2) The objective lens is adjusted until the chip and the laser spot are in focus.
- (3) The stages are moved until the light is positioned on a sensitive node of the circuit.
- (4) The laser pulse energy is increased to a level much greater than that needed to produce an upset by rotating the half-wave plate. The electronic shutter is kept open. The memory tester then supplies the address of the cell being upset.
- (5) All subsequent measurements on that cell are done by electronically strobing just that address. A "0" or a "1" is stored in the cell, the cell is irradiated, then it is read and compared to what was stored. If the information has changed, an upset is registered with a beep and the original information is again stored in the cell. A beep is more convenient than a message on a monitor.
- (6) The area most sensitive to SEE is identified by reducing the laser intensity and moving the laser spot around in the sensitive area until the location that requires the least amount of energy to upset is identified.

- (7) The next step is to determine accurately the upset threshold. Part of the light is split off by a beam splitter and its energy determined with a probe and an energy meter. The readings on the meter are recorded together with the information about whether or not an upset occurred. In this way it is a simple matter to bracket the upset threshold.
- (8) After the measurements are done, the energy meter is calibrated by measuring the energy at the location of the chip with a calibrated probe and comparing it to the value of the energy measured by the meter used during the experiment. With that information, the actual energy incident on the chip can be obtained.
- (9) The final step is to convert the energy to an LET by measuring the amount of energy lost due to reflections from the surface and subtracting that from the incident energy. The LET is then calculated by the method outlined in section 3.10.

### **4.3 System Automation**

An automated system is required for volume testing. Automation is achieved by having the computer perform as many of the tasks as possible. This would involve having the computer

- loaded with the energy range to be scanned,
- loaded with the coordinates of the regions to be tested,
- record the location of the beam,
- focus the laser beam,
- select an energy below that for upsets by rotating the half-wave plate,
- open the shutter and permit one pulse to pass,
- record the energy of the pulse,
- note whether an upset has occurred by getting the information from the tester,
- increase the energy by rotating the half-wave plate a fixed amount if no upset has occurred,
- retest for upsets,
- reduce the energy if upsets occurred, or increase the energy if none occurred,
- move to the next position, and
- repeat the measurements.

## 5. Correlation and Calibration

### 5.1 Correlation

A series of experiments on complementary metal-oxide semiconductor (CMOS) SRAMs and a bipolar logic circuit was carried out to determine whether the pulsed laser could actually give consistent and repeatable values for upset thresholds, and whether those thresholds could be correlated with ion LET thresholds. We found that the SRAMs had upset LET values (calculated from the energy deposited by the laser beam) about 50 percent higher than the equivalent ion upset LETs, whereas the bipolar logic circuits' upset values were about 35 percent higher than the values measured with an ion beam. We also found that the relative upset values of the SRAMs as measured with the laser agreed very well with the relative upset thresholds measured with an ion beam and published in the literature. This is strong evidence that the laser can be used for quantitative measurements of LET thresholds for SEE, provided a fiduciary value has been obtained with an ion beam.

For our experiments we used a series of 4K SRAMs manufactured by Harris Semiconductor and D-type flip-flops manufactured by Texas Instruments, for which ion upset data were available in the literature. The sensitive areas were large and mostly free of metal, which simplified testing. Three types of SRAMs with varying degrees of immunity to SEU and SEL were selected. They were

- HM6504—a commercial device that was not hardened to SEE,
- HM6504RH—contained epitaxial layer that eliminated SEL, and
- HM6504RRH—epitaxial layer and cross-coupled resistors that eliminated both SEU and SEL.

The laser was used to measure the upset thresholds of the four transistors in the SRAM cell. First a "0" was loaded in the cell being tested and the light focused in turn on the drains of the sensitive *n*- and *p*-channel transistors. Next, the cell was loaded with a "1" and the upset thresholds of the two remaining transistors were measured. Table 3 shows the results of our laser measurements. The upset threshold of the *p*-channel transistors was about 33 percent higher than that of the *n*-channel transistors for the HM6504. Thus, the upset value for the *n*-channel transistors determine the upset level for the circuit as a whole. The data show that the latchup level

Table 3. Upset and latchup thresholds for memory cells.

Device	Upset energy (MeV-cm <sup>2</sup> /mg)				Latchup energy (MeV-cm <sup>2</sup> /mg)	
	<i>n</i> <sub>1</sub>	<i>n</i> <sub>2</sub>	<i>p</i> <sub>1</sub>	<i>p</i> <sub>2</sub>	Cell	Periphery
HM6504	15	17	21	23	51	15
HM6504RH	54	x	x	x	No upset	No upset
HM6504RRH	195	x	x	x	No upset	No upset

is about 50 percent greater than the upset level. However, when testing the device we found that the relative latchup level of the cell was about four times greater than the reported value. We tested other parts of the circuit and found that the periphery was more sensitive to latchup than the memory cells with the relative values agreeing well with the ion data. Thus we determined that it was the periphery circuitry rather than the memory cells that dominate the SEL. Our work on the HM6504RH and HM6504RRH was not as extensive and shows only the data for one transistor in each cell. These results demonstrate the usefulness of the technique in being able to identify the location of SEE.

At this point it is only possible to speculate as to why the upset threshold measured with the laser is 50 percent higher than that measured at an accelerator. Not knowing the doping levels in the device, we were unable to quantify the role of funneling in determining the upset level. If funneling did indeed contribute to charge collection in these devices, it was expected that the laser upset threshold would be greater than the ion upset threshold.

The variations in the upset threshold from transistor to transistor and from cell to cell were due to the fact that the laser spot was not always positioned in the exact same relative position in each cell. We will discuss this point in more detail in section 6.4.

Table 4 shows the upset thresholds reported in the literature for the same device types [26]. The value for the HM6504RRH is a lower limit because ions with higher LETs and longer ranges were not available to the experimenters.

Table 5 is a compilation of all the above data after normalization to the upset levels of the HM6504 unhardened device. One sees excellent agreement between the relative values of LET thresholds measured by the ion and the pulsed laser. Furthermore, the upset values measured for different  $n$ -channel transistors in the commercial devices differed by just a few percent.

Similar measurements were carried out for the two bipolar D-type flip-flops—54ALS374 and 54S374. Table 6 shows the ion and laser data for the two devices. All six of the transistors in the 54ALS374 were tested, the most sensitive one identified, and the values noted. The same was done for the 54S374 circuit, although its layout was quite different. The results again display remarkable agreement between the relative upset values. However, the upset thresholds measured by the laser were only about 30 percent greater than the values determined by ions. The differences between the CMOS and bipolar devices may be attributed to differences in the amount of light lost through reflection, differences in doping levels, and differences between device structure. Nevertheless, the relative values are what is important and they show very good agreement.

The above results show remarkably good agreement between the relative upset levels measured by ions and laser light, suggesting that the tech-

**Table 4. Published upset and latchup LET values.**

Device	Upset energy (Mev-cm <sup>2</sup> /mg)	Latchup energy (Mev-cm <sup>2</sup> /mg)
HM6504	10	13
HM6504RH	35	No latchup
HM6504RRH	>80	No latchup

**Table 5. Comparison of ion and laser upset values.**

Device	Upset (ion)	Upset (laser)	Latchup (ion)	Latchup (laser)
HM6504	1	1	1.3	1.5
HM6504RH	3.5	3.6	No	No
HM6504RRH	>8	13	No	No

**Table 6. Ion and laser upset LETs for two bipolar devices.**

Device	Ions		Laser	
	Upset LET (MeV-cm <sup>2</sup> /mg)	Normalized values	Upset LET (MeV-cm <sup>2</sup> /mg)	Normalized values
54ALS374	5	1	6.5	1
54S374	15	3	19.6	3

nique would be suitable for SEE hardness assurance. The results also show that one cannot use the laser to determine absolute upset thresholds. A fiduciary measurement is first needed to establish the upset level against which all subsequent laser measurements can be compared.

## 5.2 Calibration

If a pulsed laser is to be used for SEE hardness assurance measurements, a calibration procedure will be required to establish a fiduciary mark against which subsequent measurements can be compared. The procedure would involve first testing a circuit for SEE with a pulsed laser to determine the upset levels. Doing the laser testing first avoids ion damage to the circuit that can affect the laser results. After the pulsed laser measurements have been done, the device should be tested at an accelerator facility with ions to determine the actual LET at which upset occurs. All subsequent laser measurements can then be compared to the ion results and any variations noted. If variations are observed, one must ascertain whether or not the variations are due to factors that affect the SEE threshold. This may be done by querying the device manufacturer for information concerning production changes, or another round of ion testing may have to be carried out. For instance, if the thickness of an oxide layer over a sensitive region changes due to a process modification, the threshold measured with the laser could be altered, whereas that measured with an ion beam would remain unchanged. Having determined the cause of the variation in the SEE threshold, we then proceeded with the laser testing.

## 6. Case Studies

We present four case studies to illustrate the usefulness of the pulsed laser for SEE testing. These four cases demonstrate the fact that the pulsed laser can provide useful information that is either difficult or impossible to obtain from accelerator testing.

In the first case [27], we tested a 64K SRAM and found

- Threshold measurements—demonstrated that one can determine cell-to-cell variations in SEU threshold.
- Spatial effects—when the beam was positioned outside a sensitive drain, upsets could still be produced, but whether an upset occurred depended on the data in the cell and the location of the laser beam. These factors affect the shape of the cross-section versus LET curve.
- Multiple upsets—the occurrence of upsets from a single laser pulse in more than one cell depended on the information stored in the cells.
- Timing effects—if the pulse arrived when the voltage on the pass transistors was high, no upsets occurred.

In the second case [3], we tested a GaAs logic circuit and found

- Timing effects—upsets occurred if the laser light arrived during a time interval just prior to the arrival of the clock signal. This time period depended on the energy of the laser and was termed “window of vulnerability.”
- Logic gate effects—not only registers but also logic gates are sensitive to upsets.

In the third case [5], we tested the registers of a logic circuit and found

- Relatively good agreement between the relative laser and ion upset thresholds.
- An “on” transistor that was sensitive to SEU by the “shunt” mechanism.

In the fourth case, we measured the cell-to-cell and intracell upset threshold uniformities in both bipolar and CMOS memory chips and found

- The intracell variation in the upset threshold is much larger than the inter-cell variation.
- The pulsed laser can be used for hardness assurance at least for devices with large open areas that permit the light to reach the sensitive junctions.

## 6.1 64K SRAM

### 6.1.1 Upset Threshold Measurements

We tested a 64K SRAM with the pulsed laser to determine the limits of the technique. The openings on the drains were comparable to the size of the beam—about 1  $\mu\text{m}$ —which meant that it was extremely important to position the spot accurately on the openings to obtain consistent results. To do this we used a computer-controlled X-Y stage with a step size of 0.1  $\mu\text{m}$ . Table 7 shows the results of upset thresholds measured for the four transistors in four different memory cells. One can see fairly good agreement from cell to cell between the corresponding upset values, suggesting the use of the pulsed laser for automated hardness assurance screening. All the values are normalized to that for the  $n_1$  transistor of cell 275. Evidently, not all the upset thresholds for the same type of transistor are the same. We did determine whether the variations in SEU thresholds measured with the laser truly reflect the actual ion SEU thresholds or if the variations are due to processing differences that affect the amount of light entering the silicon at each memory cell.

During our measurements we noticed two thresholds, a lower threshold  $E_L$  below which there were no upsets, and an upper one  $E_U$  above which there were also no upsets; i.e., upsets occurred only when the laser energy was between  $E_L$  and  $E_U$ . At the time we were unsure of an explanation and speculated that the second threshold was the result of charge diffusing over to an adjacent transistor. With energy larger than  $E_L$ , the laser light could produce an upset in, for example, the drain of a sensitive  $n$ -channel transistor. If the energy exceeded  $E_U$ , the transistor being probed would upset but some of the charge deposited in the substrate below the drain would diffuse over to the adjacent  $n$ -channel transistor, which had become sensitive following the upset of the transistor being probed. If the amount of charge that reached the drain of the adjacent transistor was sufficient, it would upset, thereby nullifying the first upset. The net result is that no upset would be detected by the tester.

The reason for this window effect was that our laser was emitting two pulses, separated in time by a few microseconds. The voltage to the flashlamps was too high and, by reducing it slightly, only a single pulse was emitted, which eliminated the effect. Thus, our explanation was essentially correct, except that it was the second pulse that produced the upset, although the mechanisms invoked—diffusion of charge to an adjacent transistor—were essentially correct. From our experience, it would be ad-

Table 7. Relative upset thresholds for transistors in four different cells in 64K SRAM.

Transistor	275	752	3775	856
$n_1$ "0"	1.0	1.0	1.1	1.1
$n_2$ "1"	1.1	1.1	1.1	1.1
$p_1$ "1"	3.0	3.1	3.8	2.8
$p_2$ "0"	3.3	3.8	3.4	2.9

visible to monitor the laser output to determine whether there are one or two pulses being emitted.

### 6.1.2 Spatial Effects

The role of charge diffusion in causing SEU was also investigated by focusing the laser spot on various positions outside the sensitive drains and increasing the energy until an upset occurred. Whether an upset actually occurred depended on both the position of the laser spot and the information stored in the cell, i.e., whether the cell contained a "1" or a "0."

Figure 6 shows the layout of the cell. The dependence of the upset threshold on both the position of the laser spot and the data loaded into two adjacent memory cells is summarized in table 8. The behavior for the two cells is complementary because, as pointed out above, even though they contain the same data, their "word" lines are interchanged so that the opposite pair of transistors is sensitive.

With the laser focused at a symmetric location (position 1) with respect to the four transistors in cell 3724, an upset was registered for a laser energy four times greater than that needed to upset transistor  $n_1$  directly when the cell was loaded with a "0." In contrast, when the cell was loaded with a

Figure 6. Layout of SRAM cell showing polysilicon lines (AA') and (BB'), drains of two  $n$ -channel and two  $p$ -channel transistors, implanted connection to  $V_{dd}$  (dotted lines), and positions where focused laser spot was placed for determining spatial dependence.

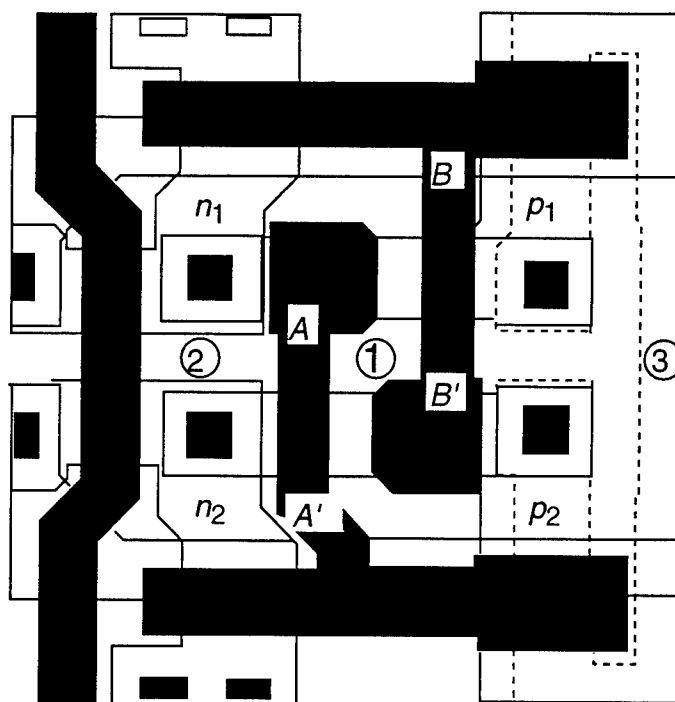


Table 8. Spatial and data dependence of upsets for two cells.

Position	Cell 3724		Position	Cell 1676	
	"0"	"1"		"0"	"1"
1	Upset	No Upset	1	No upset	Upset
2	Upset	Upset	2	Upset	Upset
3	Upset	Upset	3	Upset	Upset

"1," it did not upset, even at energies ten times higher. In this case the  $p$ -channel transistors cannot upset because they are isolated from the laser charge track by the  $n$ -well/substrate junction. Because the position of the laser is symmetrically located with respect to the two  $n$ -channel transistor drains, there should be no difference in the upset levels when the memory cell is loaded with a "0" or a "1." Evidently another factor determines whether the cell will upset, and we speculate that it is the potential on the metal interconnect that lies between the laser spot and the drains of the two transistors. That potential depends on the data in the cell. The potential gives rise to a lateral field in the low-doped  $p^-$  region that separates the electrons and holes, driving the electrons towards the drain of  $n_1$  when a "0" is written to the cell and the potential on the interconnect is high. Collection of the electrons at the drain of  $n_1$  results in an upset. Conversely, for a "1" loaded in the cell, the electric field is in the opposite direction and hinders the flow of electrons to the drain of  $n_2$ , thereby inhibiting an upset.

### 6.1.3 Multiple Upsets

Multiple upsets at higher laser energies were also observed. Figure 7 shows the physical locations of the memory cells of interest. When all the cells were loaded with "0" and the light was focused on position 1 of cell 3724, upsets occurred in cells 3724, 1676, 3716, and 1668. However, when all cells were loaded with "1" and the laser's position and energy were unchanged, upsets occurred in cells 645 and 653. Cell 3724, the one that was actually being probed by the laser light, did not upset. Significantly increasing the laser energy did not change the upset pattern.

### 6.1.4 Timing Effects

We observed timing effects when doing the upset measurements. The software used to test the circuit has, as an option, a mode in which the tester strobes only the cell being irradiated by the laser. In this mode, the tester continuously writes to the cell, reads the cell, and checks to see that the data it reads is the same as the data it wrote to the cell. If the two differ, it reports an upset by writing the address and contents of the upset to the screen and rings a bell. It then rewrites the original data. If no difference is detected, it reads the cell again. The testing cycle is controlled by the clock in the tester, which is totally separate from the laser. The clock has a frequency of about 13 Hz and the laser fires at 10 Hz.

Figure 7. Bitmap showing addresses of cells surrounding cell 3724.

2708	2700	2692	2684	2676
1684	1676	1668	1660	1652
3732	3724	3716	3708	3700
661	653	645	637	645
2709	2701	2693	2685	2677

When testing a particular transistor in the memory cell, we noticed that at times the cell would not upset, in spite of the fact that the amount of energy deposited in the sensitive area was well above that needed to produce an upset. We suspected that this may occur if the laser pulse arrives when the pass transistors are conducting during reading or writing of the cell. With the pass transistors conducting, a large capacitance is added to the sensitive node being tested that "sinks" the charge generated by the laser light and so inhibits upsets. Because the circuit clock and the laser were not synchronized, the effect occurred only when the laser pulse arrived at the same time the pass transistors were conducting.

This explanation was confirmed by an experiment in which we wrote to the cell, irradiated it with the laser, and then read it in sequence. At no time did a pulse of laser light arrive when the transistors were turned on. Using this method, we were unable to observe any pulses larger than the threshold that did not cause upset.

In conclusion, we have demonstrated that the laser can be used to test 64K SRAMs for SEU sensitivity, and that one can obtain a great deal of information on timing sensitivity issues.

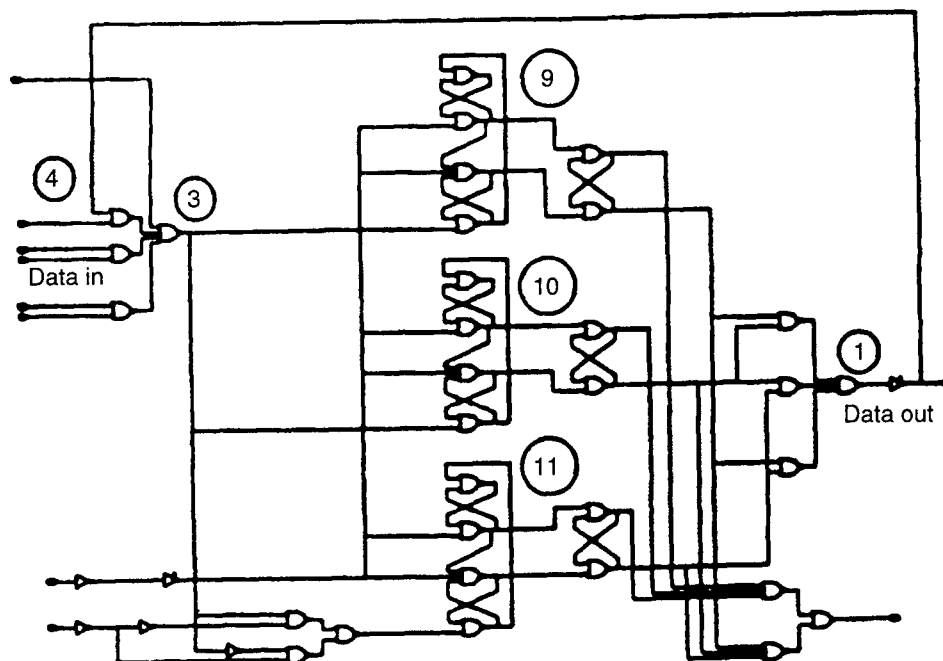
## 6.2 GaAs Logic Circuit

The usefulness of the pulsed laser for SEE testing is illustrated by a study we performed of upsets generated in a GaAs logic circuit. The circuit was manufactured using 1.25- $\mu\text{m}$  MESFET technology that is known to be very sensitive to SEU, with an upset threshold of 1 MeV-cm<sup>2</sup>/mg [28]. The GaAs logic design was implemented to show that replacing silicon circuits with GaAs circuits in a computer destined to be operated in space would reduce the computer's size and weight and also increase its speed. At the time the circuit was being designed, it was believed that it was necessary to harden only the registers where the data was stored for relatively long periods of time. No effort was made to harden any other part of the circuit.

An initial design consisted of some test structures that were evaluated both with an ion beam and a pulsed laser beam to determine the critical charge for upset. Modeling was also done to determine the critical charge theoretically. The critical charge obtained from ion-beam testing was 64 fC, and from pulsed laser testing it was 60 fC. The theoretical value was 48 fC. Both the ion and laser data indicated a very small critical charge, meaning that the registers would be very sensitive to upsets if no measures were taken to harden them.

Because the registers were so sensitive to upsets, special designs were incorporated to improve their SEU immunity. Figure 8 shows the layout of the circuit in which the data are stored in pipeline registers 1, 2, and 3. The scheme involved writing each bit of data into three identical pipeline registers that were physically separated from each other to minimize the probability of a single ion producing upsets in more than one of the registers. The data were majority voted on each clock cycle and the output fed back

Figure 8. Schematic of one pipeline register designed for SEU immunity by using majority voting and scrubbing.



into the input. The gates in the feedback loop are marked 4 to 9. Hence, if an upset occurred in a single register, the output would still be valid and upon rewriting the data, the disturbed data in would be corrected. However, if two cells upset, the data would be incorrect. By rewriting the data into the registers on every clock cycle, the data would, presumably, be corrected before two of the three registers upset. Thus, for sufficiently high fluxes, two upsets could occur at low clock frequencies, and the problem could be eliminated merely by increasing the frequency. Therefore, at high fluxes, the number of upsets should decrease as the frequency increases.

Tests at Brookhaven National Laboratory did indeed show that as the frequency increased, the number of upsets decreased. However, above a certain frequency that depended on the flux, the number of upsets started to increase with frequency. Apparently, some other mechanism is responsible for those upsets.

The pulsed laser was used to test not only the registers, but also all other possible sensitive gates that might be the source of upsets. Results indicate that all the gates in the feedback path are sensitive to upset because the feedback loop is connected to the inputs of all three registers. However, those gates are only sensitive to upset if the pulse arrived just before the clock voltage switched from low to high. If it arrives after the clock has switched, no upsets occur. For our original measurements, the clock and the firing of the laser were not synchronized. Therefore, a long time was needed to measure the threshold, because upsets occurred only when the laser arrived just as the clock voltage was switching.

In order to measure the exact time during which the nodes in the feedback loop are sensitive, we used a trigger from the laser to trigger the clock and varied the delay between the laser pulse and the clock. Because the jitter in

the timing was much less than a nanosecond, we were able to get accurate measurements of upset threshold with respect to time. We found that the earlier the laser light arrived with respect to the clock voltage toggling from low to high, the greater the energy needed to produce an upset. If the light arrived after the clock had toggled, no upset would occur. Figure 9 shows a plot on semilog paper of the energy required to produce an upset versus the time between the arrival of the laser pulse and the clock signal. The data fall on a straight line, the slope of which gives the charge collection time. In fact, these results revealed for the first time the presence of a time window for upsets that varies in width with LET. Thus, particles with higher LET will more likely produce an upset, not only because the charge deposited is larger than the minimum needed to produce an upset, but also because the relative amount of time the gate is vulnerable increases with LET. Figure 9 also shows the width of the window for a particular value of LET.

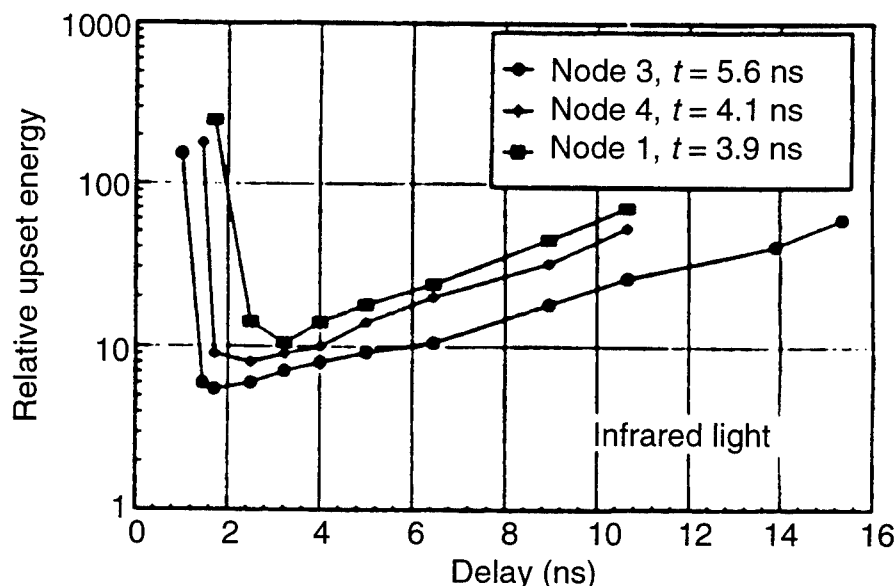
The above two examples demonstrate how useful the pulsed laser can be for SEE testing of integrated circuits. We have shown that the pulsed laser can play a significant role in the testing of logic circuits, largely because of the spatial and temporal information it can provide.

### 6.3 SA3300 Microprocessor

The SA3300, a radiation-hardened CMOS implementation of the National Semiconductor 16-bit microprocessor, is the basis for the SPACE-16 computer that will be used in the CRAG and CASSINI space probes. It was designed to withstand severe radiation environments, including SEU. Two versions of the processor were manufactured and tested; "Rev A" had transistors with 2- $\mu\text{m}$  channel lengths, and "Rev B"  $n$ - and  $p$ -channel transistors had channel lengths of 1.75 and 1.25  $\mu\text{m}$ , respectively.

Because SEUs in logic circuits depend on software and are difficult to characterize, SEU testing of the SA3300 was limited to measuring upset thresh-

Figure 9. Relative upset threshold as function of delay between arrival of laser pulse and arrival of clock for three nodes of pipeline register.

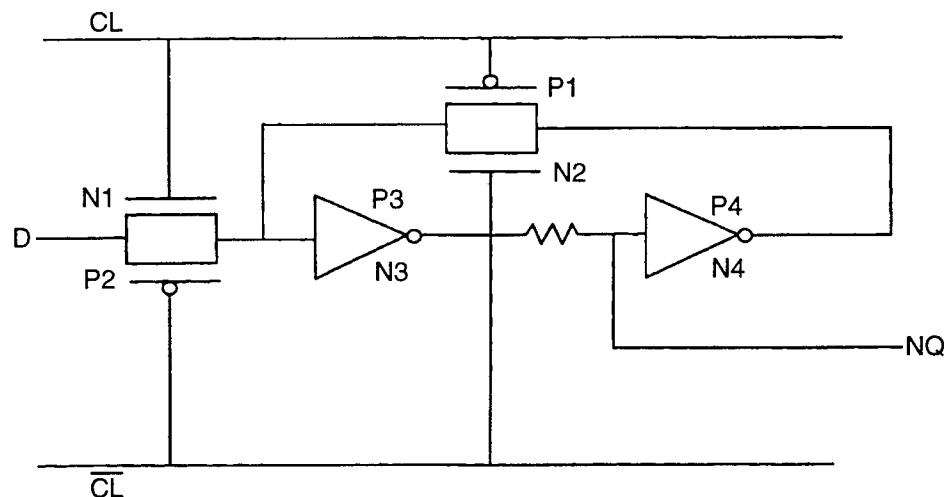


olds in the general-purpose registers. Ion data showed that the upset threshold for Rev A registers filled with "1's" was much lower ( $35 \text{ MeV-cm}^2/\text{mg}$ ) than when they were filled with "0's" ( $83 \text{ MeV-cm}^2/\text{mg}$ ). Upset thresholds for registers in Rev B exhibited a smaller asymmetry and lower values.

The pulsed laser was used to investigate the origins of the asymmetry. Figure 10 shows the design of a register that consists of two pass gates (N1/P1 and N2/P2) and two inverters (N3/P3 and N4/P4). D is data input and NQ is data output. The sensitive nodes are the drains of the "off" transistors. When a "1" is stored in the register, NQ is high (P1, P4, and N3 are sensitive), whereas when a "0" is stored, P3, N1, and N4 are sensitive. The low threshold observed in the "1's" state cannot be accounted for by strikes at either nodes N3 or P4 because their potentials are easily restored through P3 and N4, respectively. P1 was expected to be more sensitive to upsets than either N3 or P4 because node A is restored through the passgate formed by transistors N2 and P2. This was confirmed by the laser data. Surprisingly, the laser data indicate that the "on" drains of transistors N1 and N2 were more sensitive than the "off" drain of P1. Therefore, a different mechanism was invoked to explain upsets in N2. One possible mechanism was a positive-going photocurrent pulse generated in a vertical  $n^+pn$  bipolar transistor formed by the  $n$ -channel source/drain regions, the  $p$ -well, and the underlying epilayer. This type of mechanism was previously observed and termed the "shunt" effect. Because the computer code used to model upsets in the latch showed that strikes to N2 required three times more energy than strikes to N3 and P4, additional work needs to be done. In particular, these results suggest that the model of the shunt effect on which the computer code is based needs to be refined to more accurately predict upset levels involving the shunt effect.

The upset thresholds measured with ions are established by the upset levels of the most sensitive transistors when a "0" or a "1" is stored in the latch. With a "1" is stored in the register, the most sensitive transistor is N2, and with a "0" is stored in the latch, the most sensitive transistor is P1. As previously pointed out, the laser does not give reliable absolute values

Figure 10. Schematic of register for SA3300 microprocessor.



of upset threshold. However, the relative upset thresholds were compared with the ion data. Table 9 shows the upset levels for both ions and the laser with the laser data for "1" in Rev B set at the same value as the ion data. All other data are scaled accordingly. Except for "0" stored in Rev B, the relative values for the laser and the ion exhibit remarkable agreement. The discrepancy for zero stored in Rev B was not investigated further.

## 6.4 Spatial Variation in Upset Threshold

We used the pulsed laser to investigate the intracell and the cell-to-cell variations in the upset thresholds for two different types of memory cells—a  $256 \times 4$  bipolar SRAM (93L422) and a 4K CMOS SRAM (HM6504RRH). The goal of this work was twofold: first, to identify the origins of the gradual rise in the cross-section versus LET curve and, second, to assess the laser for hardness assurance applications.

The 93L422 has large memory cells designed so that the collector covers almost the entire cell. Using the laser, we found that one half of a cell is sensitive when it contains a "0," and the other half is sensitive when it contains a "1." Furthermore, we determined that when all the memory cells were loaded with the same data, the SEE-sensitive region in each row was the mirror image of that in an adjacent row. Thus, the sensitive regions were alternately separated by either just over a micron or by the width of two cells—more than  $100 \mu\text{m}$ .

Figure 11 shows the distribution of the upset thresholds for 102 cells for which the laser spot was positioned on exactly the same relative position in each cell. The results show that there is a clear bimodal distribution in upset threshold, peaked at pulse energies of 206 and 235, a difference of 15 percent. The lower upset threshold applied to odd rows and the upper to even rows. Evidently, the cells are not exactly symmetrical. The standard deviation is 3.76 for the lower and 7.2 for the upper thresholds showing that the variation in upset threshold is less than 5 percent of the actual value. Figure 12 shows that the cross-section versus LET curve rises gradually over more than an order of magnitude in LET, suggesting that the cell-to-cell variation cannot explain the dependence of cross-section on LET. In fact, analysis shows that the variation would have to be about 200 percent in order to account for the gradual rise in cross-section. On the other hand, the intracell upset threshold exhibited a large spatial variation, large enough to account for the shape of the cross-section versus LET curve.

**Table 9.** Upset thresholds ( $\text{MeV}\cdot\text{cm}^2/\text{mg}$ ) for ion and laser tests on Rev A and Rev B versions SA3300.

Logic state	Rev A		Rev B	
	Ion	Laser	Ion	Laser
1's	35	30	23	23
0's	83	95	30	54

*Upset value for 1's stored in Rev B registers and measured with laser was scaled to ion value. All other values were scaled accordingly.*

Figure 11.  
Distribution of upset  
threshold for 93L422.

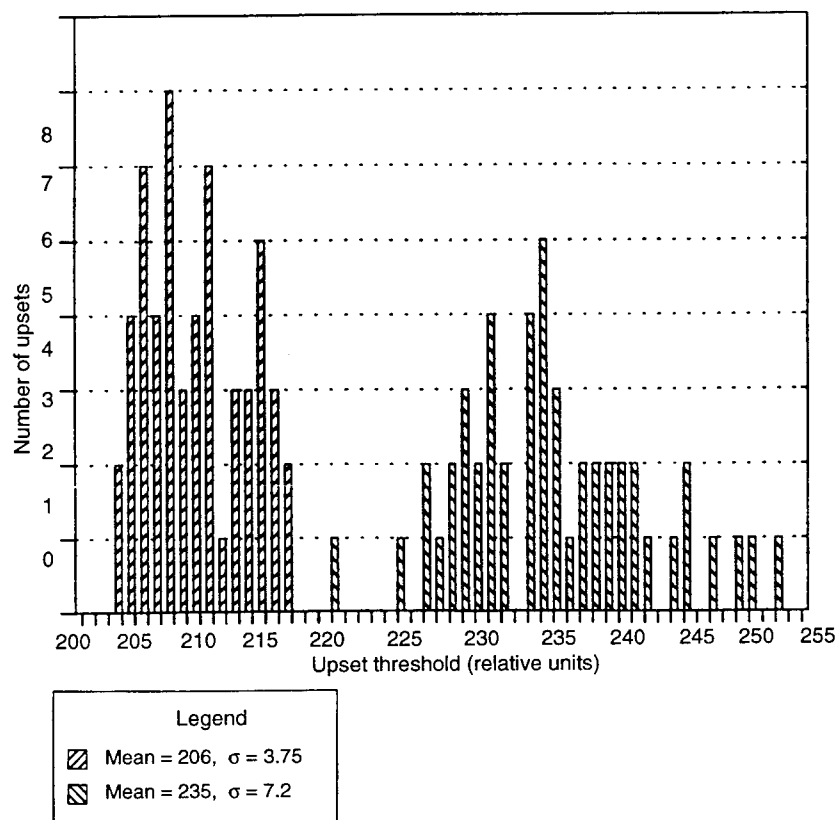
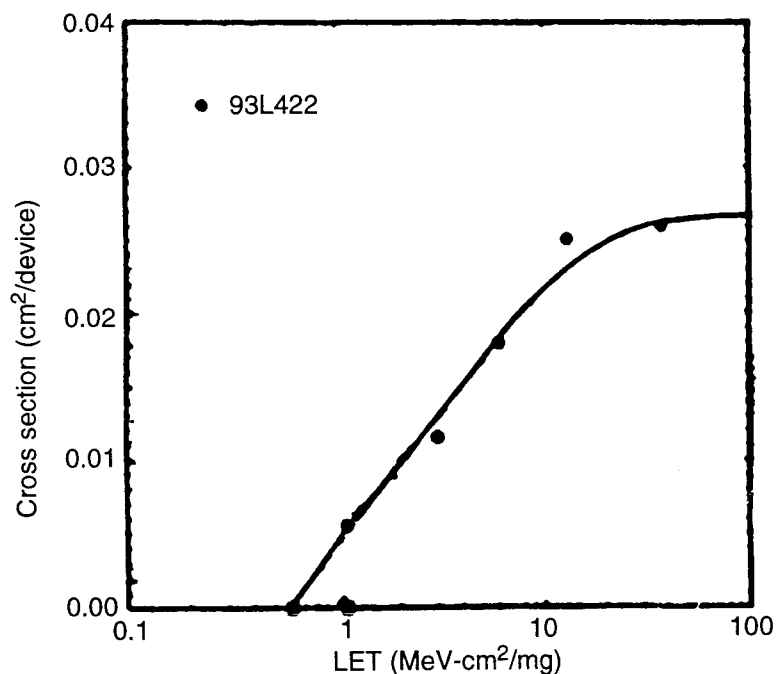


Figure 12. Cross-section as function of LET for 93L422, showing gradual rise of cross-section with LET.



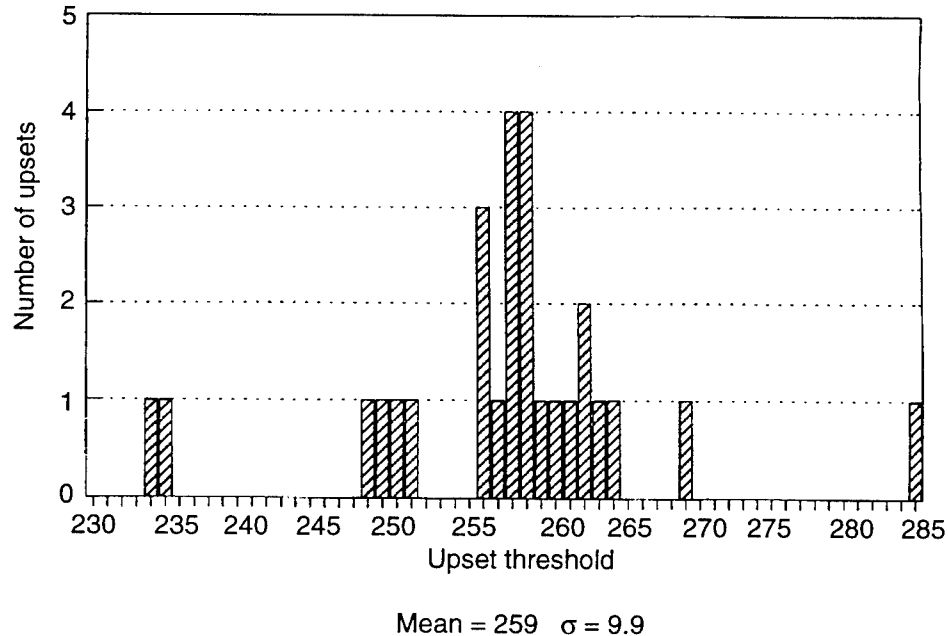
For comparison purposes, the HM6504RRH was also tested for upset uniformity because a previous report had claimed that the upset threshold varied significantly across the chip due to difficulty in maintaining uniformity across chips of the resistance of polysilicon decoupling resistors [7].

The chip manufacturer assured us that the uniformity problem had been solved, and our results agree with their prediction. Figure 13 shows the values of the upset thresholds. Their average energy for upset was 259 (arbitrary units) with a standard deviation of 9.9, which is a 3.8 percent variation in the cell-to-cell upset threshold. Within the drain itself, we found a much larger variation (from 261 to around 500) than the cell-to-cell variation. The intracell variation in the case of the HM6504RRH is significantly less than that observed for the 93L422, and this result is consistent with the much sharper rise in the cross-section versus LET curve for the HM6504RRH.

The fact that consistent results could be obtained for cell-to-cell upset thresholds if the identical location is selected in each cell, implies that the pulsed laser can be used for hardness assurance measurements. It should be noted that these results are for memories where the sensitive areas are much larger than the beam size. It has not yet been determined whether the technique could be used for devices where the open areas are smaller or comparable to the size of the beam. Further work in this regard should be undertaken.

These results demonstrate that the laser is a useful tool for uncovering SEU phenomena, such as the presence of the shunt effect, and is also capable of providing relative upset thresholds.

Figure 13.  
Distribution of upset  
thresholds for  
HM6504RRH SRAM.



## 7. Lessons Learned

From our experience testing numerous circuits for SEE, we have distilled the following lessons:

- A good understanding of the circuit layout and operation is essential for doing measurements with the pulsed laser. SRAMs are not too complicated to decipher without a diagram of the layout. However, logic circuits contain many different functional components that must be understood before testing can be done.
- Circuits with large open areas free of metal are easy to test because it is simple to position the laser on the sensitive area. Circuits with sensitive areas covered by metal can still be tested by placing the beam next to the sensitive area. However, upset thresholds cannot be accurately measured using this technique.
- The laser should be checked for proper operation, i.e., it should emit only one pulse that has a pulse width much shorter than the response time of the circuit.
- A great deal of electromagnetic noise is emitted by the power supply for some Q-switched lasers, which may interfere with the measurements. Care should be taken to isolate the noise by using some form of Faraday cage, or by using short shielded cables.

## 8. Perspectives

A combination of ion beams, pulsed lasers and Californium is perhaps the ideal way of doing SEE testing. The main disadvantage of Californium is that the ions emitted have a small range and, therefore, are limited with respect to SEL testing. Lasers and accelerators can supply complementary information about SEE in integrated circuits. A laser will never replace accelerator testing, but it can be used as a diagnostic tool and for SEE hardness assurance. The laser's usefulness may be limited as the minimum feature size of circuits decreases.

Circuits must be designed with open areas on sensitive transistors if SEE testing is anticipated. This may be difficult to achieve, given the complexity of current circuits that contain multilevel metal interconnects.

Pulsed lasers will find use in

- diagnostic testing,
- hardness assurance testing,
- testing of multichip modules covered with thick dielectrics,
- generating bit maps for understanding multiple upset,
- charge-collection measurements,
- time-dependent effects,
- testing circuits with large upset thresholds ( $>100 \text{ MeV-cm}^2/\text{mg}$ ),
- validation of EDAC schemes, and
- validation of software used for identifying SEE before accelerator testing.

The biggest potential for pulsed-laser testing is for logic circuits that contain many different functional components whose SEE sensitivity depends on their dynamic state. It will also be of tremendous use in multichip modules that cannot be tested with ion beams because of the thick dielectric layer that covers the chip and prevents accelerator ions from reaching the circuit.

The effects of such mechanisms as two-photon absorption, free-carrier absorption, and bandgap renormalization can be neglected if one selects the appropriate wavelength.

The pulsed laser does not give accurate values for the upset thresholds because the charge tracks produced by ions and by laser beams are very different. In addition, the upset threshold varies spatially in the sensitive areas, and the location of the area most sensitive to upsets may be obscured by metallization.

## 9. Conclusions and Recommendations

### 9.1 Conclusions

From the above discussion, one can conclude that the pulsed laser is a very useful technique for SEE evaluation of integrated circuits, particularly for

- hardness assurance where changes in upset levels can easily and inexpensively be measured;
- diagnostic tests in circuits that do not exhibit the expected SEU upset level, particularly circuits with special designs for enhancing SEU immunity;
- testing of logic circuits for isolating the locations of SEUs and their dependence on the code being used; and
- testing multichip modules that cannot be tested with an ion beam because of the thick dielectric layer covering the circuit.

However, pulsed-laser testing will not replace ion-beam testing completely because

- the pulsed laser cannot be counted on to provide accurate LET threshold values for a circuit without the ion data;
- some circuits with multilevel metal interconnects have all their sensitive nodes obscured with metal, making it difficult to probe the circuit with light; and
- as the minimum dimensions of circuits drop below 1  $\mu\text{m}$ , reliable measurements will be more difficult with a beam having a diffraction-limited diameter of 1.0  $\mu\text{m}$ .

### 9.2 Recommendations

Our recommendations are

- Manufacturers of SEE-immune integrated circuits should have a pulsed laser testing facility available for routine testing of parts. The cost is not great (~\$135K), and it can save expense and time by avoiding some accelerator testing.
- To facilitate pulsed-laser testing, every effort should be made to design the circuits with the sensitive nodes as free of metal as possible.
- The system should be automated to reduce the tedium of taking measurements.
- A person knowledgeable in running a pulsed laser system should be in charge of the equipment, making sure that the laser is in proper operating condition.

## 10. References

1. C. Dufour, P. Garnier, T. Carriere, J. Beaucour, R. Ecoffet, and M. Labrunee, *Heavy Ion Induced Single Hard Errors on Submicronic Memories*, IEEE Trans. Nucl. Sci. **NS-39** (1992), 1693.
2. T. R. Oldham, K. W. Bennett, J. Beaucour, T. Carriere, C. Polvey, and P. Garnier, *Total Dose Failure in Advanced Electronics from Single Ions*, IEEE Trans. Nucl. Sci. **NS-40** (1993), 1820.
3. H. Dussault, J. W. Howard, R. C. block, M. R. Pinto, W. J. Stapor, and A. R. Knudson, *Numerical Simulation of Heavy Ion Charge Generation and Collection Dynamics*, IEEE Trans. Nucl. Sci. **NS-40** (1993), 1926.
4. A. H. Johnston and B. W. Hughlock, *Latchup in CMOS from Single Particles*, IEEE Trans. Nucl. Sci. **NS-37** (1990), 1886.
5. S. Buchner, K. Kang, W. J. Stapor, A. B. Campbell, A. R. Knudson, P. McDonald, and S. Rivet, *Pulsed Laser-Induced SEU in Integrated Circuits: A Practical Method for Hardness Assurance Testing*, IEEE Trans. Nucl. Sci. **NS-37** (1990), 1825.
6. R. Schneiderwind, D. Krening, S. Buchner, K. Kang, and T. Weatherford, *Laser Confirmation of SEU Experiments in GaAs MESFET Combinational Logic*, IEEE Trans. Nucl. Sci. **NS-39** (1992), 1665.
7. R. A. Kohler and R. Koga, *SEU Characterization of Hardened CMOS SRAMS using Statistical Analysis of Feedback Delay in Memory Cells*, IEEE Trans. Nucl. Sci. **NS-36** (1989), 2318.
8. S. Buchner, W. J. Stapor, J. Langworthy, and A. B. Campbell, *Implications of the Spatial Dependence of the Upset Threshold of the 93L422 SRAM Measured with a Pulsed Laser*, presented at the 1994 NSREC, Tuscon, AZ (22 July 1994).
9. Q. Kim, H. Schwartz, K. McCarty, J. Coss, and C. Barnes, *Single Event Effects on Space Radiation Hardened 64K SRAMs at Room Temperature*, IEEE Trans. Nucl. Sci. **NS-40** (1993).
10. E. J. Kobetich and R. Katz, *Energy Deposition by electron Beams and Delta Rays*, Phys. Rev. **170** (1968), 391.
11. F. B. McLean and T. R. Oldham, *Charge Funneling in N- and P-Type Si Substrates*, IEEE Trans. Nucl. Sci. **NS-39** (1982), 2018.
12. S. Buchner, A. R. Knudson, K. Kang, and A. B. Campbell, *Charge Collection from Focussed Picosecond Laser Pulses*, IEEE Trans. Nucl. Sci. **NS-35** (1988), 1517.

13. F. W. Sexton, R. K. Treece, K. J. Hass, K. L. Hughes, G. L. Hash, C. L. Axness, S. P. Buchner, and K. Kang, *SEU Characterization and Design Dependence of the SA3300 Microprocessor*, IEEE Trans. Nucl. Sci. **NS-37** (1990), 1861.
14. Private communication with H. Dussault (20 April 1994).
15. E. C. Finch, M. Ashgar, and M. Forte, *Plasma and Recombination Effects in the Fission Fragment Pulse Height Defect in a Surface Barrier Detector*, Nucl. Instrum. and Meth. **163** (1979), 467.
16. E. C. Finch, *an Analysis of the Causes of the Pulse Height Defect and its Mass Dependence for Heavy-ion Silicon Detectors*, Nucl. Instrum. and Meth. **113** (1973), 41.
17. M. Martini, J. W. Mayer, and K. R. Zanio, *Drift Velocity and Trapping in Semiconductor Transient Charge Technique*, Applied Solid State Science **3**, Academic Press (1972), 181.
18. C. A. Gossett, B. W. Hughlock, and A. H. Johnson, *Laser Simulation of Single Particle Effects*, IEEE Trans. Nucl. Sci. **NS-39** (1992), 1647.
19. R. Wagner, N. Bordes, J. M. Bradley, C. J. Maggiore, A. R. Knudson, and A. B. Campbell, *Alpha-, Boron-, Silicon-, and Iron-Ion-Induced Current Transients in Low-Capacitance Silicon and GaAs Diodes*, IEEE Trans. Nucl. Sci. **NS-35** (1988), 1578.
20. M. Saritas and H. D. McKell, *Absorption Coefficient of Si in the Wavelength Region Between 0.80 - 1.16  $\mu\text{m}$* , J. Appl. Phys. **61** (1987), 4923.
21. R. Koga, S. D. Pinkerton, S. C. Moss, D. C. Mayer, S. LaLumondiere, S. J. Hansel, K. B. Crawford, and W. R. Cain, *Observation of Single Event Upsets in Microcircuits*, IEEE Trans. Nucl. Sci. **NS-40** (1993), 1838.
22. A. H. Johnston, *Charge Generation and Collection in p-n Junctions Excited with Pulsed Infrared Lasers*, IEEE Trans. Nucl. Sci. **NS-40** (1993), 1694.
23. J. P. Woerdman, Phillips Res. Rept. Suppl. 7 (1971).
24. P. E. Schmidt, *Optical Absorption in Heavily Doped Silicon*, Phys. Rev. **B 23** (1981), 5531.
25. H. C. Casey, D. D. Sell, and K. W. Wecht, *Concentration Dependence of the Absorption Coefficient for n- and p-Type GaAs Between 1.3 and 1.6 eV*, J. Appl. Phys. **46** (1975), 250.
26. R. Koga and W. A. Kolasinski, *Heavy Ion-Induced Single Event Upsets of Microcircuits; A Summary of the Aerospace Test Data*, IEEE Trans. Nucl. Sci. **NS-31** (1984), 1190.

## Distribution

Admnstr  
Defns Techl Info Ctr  
Attn DTIC-DDA (2 copies)  
Cameron Sta Bldg 5  
Alexandria VA 22304-6145

Director  
Defns Nuc Agcy  
Attn RAEE L Cohn  
6801 Telegraph Rd  
Alexandria VA 22310-3398

Commanding Officer  
Nav Weapons Spprt Ctr  
Attn Code 6054 D Platteter  
Attn Code 6054 T Turflinger  
Bldg 2088  
Crane IN 47522

Naval Rsrch Lab  
Attn Code 6613 A Campbell  
Attn Code 6613 W Stapor  
Attn Code 6680 D Brown  
Washington DC 20375-5345

Phillips Lab  
Attn M A Shea  
29 Randolph Rd Hanscom AFB  
Bedford MA 01731-3010

Phillips Lab  
Attn T Ihringer  
3550 Aberdeen Ave SE  
Albuquerque NM 87117

Rome Lab  
Attn ERDA W Dussault  
525 Brooks Rd  
Griffis AFB NY 13441-4505

Sandia National Lab  
Attn MS 1083 F W Sexton  
Attn Div 1332 P Winokur  
PO Box 5800  
Albuquerque NM 87185-1083

NASA/GSFC  
Attn Code 735.1 K A Label  
Attn E G Stassinopoulos MS 900  
Goddard Space Flight Ctr  
Greenbelt MD 20771

Clemson Univ  
Attn P J McNulty  
117 Kinard Lab  
Clemson SC 29634-1911

Johns Hopkins Univ Applied Physics Lab  
Attn R Maurer  
Johns Hopkins Rd  
Laurel MD 20723-6099

Vanderbilt Univ Dept of Elec Eng  
Attn L M Massengill  
PO Box 69-B  
Nashville TN 37235

Arspec Corp  
Attn MS M2-259 R Koga  
Attn MS M2-253 S Moss  
Attn M5/653 L Mendoza  
PO Box 29257  
Los Angeles CA 90009-2957

Boeing Defense & Space  
Attn MS 9F-51 M P Baze  
Attn MS 9f-51 W Bartholet  
PO Box 3999  
Seattle WA 98124-2499

California Inst of Techlgy Jet Propulsion Lab  
Attn MS-303/220 C Barnes  
4800 Oak Grove Dr  
Pasadena CA 91109

Computing Devices Int'l  
Attn D Newberry MS BLCS1P  
8800 Queen Ave S  
Bloomington IN 55431

## Distribution

Consultant  
Attn E C Smith  
PO Box 880  
Monteagle TN 37356

Consultant  
Attn S Buchner  
4205 Bright Bay Way  
Ellicott City MD 21042

Consultant  
Attn E Petersen  
9502 Babson Ct  
Fairfax VA 22032

Hughes Aircraft Co  
Attn MS Bldg S41/B366 M A Shoga  
PO Box 92919  
Los Angeles CA 90009

Jaycor  
Attn S C Rogers  
9775 Towne Centre Dr #3075  
San Diego CA 92128-5154

Jet Propulsion Lab  
Attn MS 303-220 A Johnston  
4800 Oak Grove Dr  
Pasadena CA 91109

Jet Propulsion Lab California Inst of Techlgy  
Attn D J Nichols T-1180  
Pasadena CA 91103

Messenger & Assoc  
Attn G Messenger Ste 7-F  
3111 Bel Air Dr  
Las Vegas NV 89109

Rockwell  
Attn MS 272 FB66 V Strahan  
3370 Miraloma Ave  
Anaheim CA 92669

Rsrch Triangle Inst  
Attn M Simons  
PO Box 12194  
Research Triangle Park NC 27709

S-Cubed  
Attn J C Pickel  
27001 La Paz Rd Ste 400  
Mission Vieho CA 92691

US Army Rsrch Lab  
Attn AMSRL-CI DE  
Attn AMSRL-OP-SD-TA Mail & Records  
Mgmt  
Attn AMSRL-OP-SD-TL Tech Library  
(3 copies)  
Attn AMSRL-OP-SD-TP Tech Pub  
Attn AMSRL-SL DE  
Attn AMSRL-SS DE  
Attn AMSRL-WT Chf  
Attn AMSRL-WT DE  
Attn AMSRL-WT-A Chf  
Attn AMSRL-WT-EH Chf  
Attn AMSRL-WT-N Chf  
Attn AMSRL-WT-N Dpty Chf  
Attn AMSRL-WT-NA Chf  
Attn AMSRL-WT-NB Chf  
Attn AMSRL-WT-NC Chf  
Attn AMSRL-WT-ND Chf  
Attn AMSRL-WT-NE Chf  
Attn AMSRL-WT-NF Chf  
Attn AMSRL-WT-NG Chf  
Attn AMSRL-WT-NG H Eisen  
Attn AMSRL-WT-NG T Oldham  
Attn AMSRL-WT-NH Chf  
Attn AMSRL-WT-NI Chf  
Attn AMSRL-WT-NJ Chf  
Attn AMSRL-WT-P Chf  
Attn AMSRL-WT-T Chf  
Attn AMSRL-WT-W Chf  
Attn AMSRL-WT-PB Chf  
Attn AMSRL-WT-WB Chf  
Attn AMSRL-WT-WC Chf  
Attn AMSRL-WT-WD Chf